JOURNAL OF THE AERONAUTICAL SCIENCES

VOLUME 10 MARCH, 1943 NUMBER 3

Maneuverability Criteria Through Turning Performance*

JOHN E. GOODE, JR.†

Douglas Aircraft Company, Inc.

SUMMARY

A method has been developed which makes possible the determination of the transition time for an airplane to maneuver into steady turning flight from a level straight-line course and the control deflections necessary to execute this maneuver. Accelerations encountered are easily obtained from data necessary to compute the maneuvering time. The method developed is based on the six fundamental stability equations. The major assumptions are angles of bank, Φ, and no sideslip during turn, i.e., $v = 0$. Only the use of conventional wind-tunnel data is necessary.

Calculations are presented for a typical twin-engined attack bomber. The effect of mass distribution is shown by considering a modified single-engined airplane of the same weight and horsepower as that of the twin-engined design. The bank assumption chosen produced a helix angle of 0.090 and maximum bank of 75°. Calculations were carried out for sea level and for 15,000 ft. altitude.

From the standpoint of practical application, the method developed presents not only a means of estimating the maneuvering characteristics of a particular airplane but offers a basis for comparison of similar airplanes, since control deflections necessary to effect a given maneuver are available as a function of time. This is illustrated in the calculations worked out for the two airplanes mentioned above. The time to maneuver from straight and level flight into a steady turn is substantially the same at sea level and 15,000 ft., but at high altitude the control deflections required for the twin-engined airplane exceed those necessary for the modified single-engined one. As suspected, this shows that an increase in spanwise mass distribution is detrimental to the maneuvering characteristics of an airplane.

INTRODUCTION

THE IMPROVEMENT of the flying qualities of modern aircraft is impeded by the absence of quantitative maneuverability and control criteria.[1] Wing loading, span loading, power loading, altitude, and speed are all factors influencing the behavior of the aircraft. To get a concise maneuverability criteria that takes into account all these variables is extremely difficult, and no attempt has been made to do so in this report.

As a special definition of maneuverability, the airplane was arbitrarily assigned a flight path, and equations were worked out to give the time necessary to execute the maneuver as well as the control motions.

The flight path chosen was that executed by the airplane in going from straight and level flight into a steady turn. For necessary simplification, application of constant power was maintained throughout the turn. This phase of maneuverability is of great importance in the case of a night fighter plane when it is in pursuit only by instrument and when a rapid turn at full power may be necessary. The basic assumption for this designated flight path was the rate of change of angle of bank with time. This relationship was taken as an exponential function.

Calculations are worked out for a typical, modern, twin-engined bomber, and the effect on maneuverability of engines mounted in the wing is shown by considering the airplane single-motored, the motor being mounted in the fuselage, having the same weight, and developing the same horsepower as the two engines installed in the wing of the initial airplane.

Methods presented in this paper are based on the interpretation of wind-tunnel data that should always be available, at least in preliminary form, during the design stages of aircraft on which rational analysis is important. All curves have been calculated for a conventional airplane of about 20,000 lbs. gross weight. Although the above magnitude is of no particular significance, the general trends and relationships should hold for airplanes of twice and half this size.

Outside of general specifications and speed conditions, the only factors necessary are:

Presented at the Aerodynamics Session, Eleventh Annual Meeting, I.Ae.S., New York, January 25–29, 1943.

* Revised copy of thesis presented in partial fulfillment of the requirements for the professional degree in Aeronautical Engineering, California Institute of Technology, 1942.

† Member, Stability and Control Group in the Aerodynamics Section.

Y_{0_r} = change in side force per unit mass due to unit rudder deflection
L_{0_r} = change in rolling moment per unit moment of inertia due to unit aileron deflection
N_{0_r} = change in yawing moment per unit moment of inertia due to unit rudder deflection
N_{0_a} = change in yawing moment per unit moment of inertia due to unit aileron deflection
L_r = change in rolling moment due to yawing velocity
L_p = change in rolling moment due to rolling velocity
N_r = change in yawing moment due to yawing velocity
N_p = change in yawing moment due to rolling velocity

Basic Equations and Assumptions

Because of the bilateral symmetry of the airplane it is customary to divide the motions into two independent groups—the lateral and the longitudinal—each consisting of three degrees of freedom: (1) lateral motions —(a) rolling, (b) yawing, (c) sideslipping; and (2) longitudinal motions—(a) pitching, (b) vertical translation, (c) forward translation.

Presumably, the reactions to small increments of longitudinal speed or displacement do not sensibly influence the lateral motions and the two groups may be treated independently.

The Lateral Motions

If the flight path is assumed to be horizontal (or nearly so) and the main forward velocity U_0 to be substantially constant, the equations of motion in a lateral disturbance may be written:[2]

(In sideslipping) $dv/dt = g \sin \Phi - rU_0 + vY_v + Y_0$
(In rolling) $dp/dt = vL_v + pL_p + rL_r + L_0$
(In yawing) $dr/dt = vN_v + pN_p + rN_r + N_0$

The quantities that arise in the consideration of the lateral motions are defined in *N.A.C.A. T.R. No. 560* and are in keeping with standard N.A.C.A. convention.

It has been found convenient to transform all stability derivatives and disturbing effects into terms of accelerations of the airplane rather than retaining them as moments and forces. This transformation is accomplished by dividing out the appropriate moments of inertia and the mass of the airplane. For example,

$(\partial L/\partial p)/mK_x^2$ may be written simply as L_p; similarly, $(\partial N/\partial v)/mK_x^2 = N_v$ and $(\partial Y/\partial r)/m = Y_r$.

On the basis of these definitions the above equations for sideslipping, rolling, and yawing were written. Since the axes chosen will ordinarily lie near the axes of the principal moments of inertia of the airplane, terms involving the products of inertia have been neglected.

Solution of the Lateral Equations

From the three lateral equations, the unknowns are Φ, r, v, Y_0, L_0, N_0.

One of the unknowns can be eliminated by letting

$$Y_0 = \delta_r Y_{0_r}$$
$$L_0 = \delta_a L_{0_a}$$
$$N_0 = \delta_r N_{0_r} + \delta_a N_{0_a}$$

For the two other unknowns: (1) specify Φ; (2) specify v.

Taking $v = 0$ (as suggested in *N.A.C.A. T.R. No. 560*) and assuming

$$\Phi = k\left(\frac{1 - e^{-nt}}{n} - \frac{1 - e^{-(n+m)t}}{n+m}\right)$$

the three equations of lateral motion may now be written:

$$rU_0 - \delta r Y_{0_r} = g \sin \Phi \tag{1}$$

$$rL_r + \delta_a L_{0_a} = (dp/dt) - pLp \tag{2}$$

$$(dr/dt) - rN_r - \delta_r N_{0_r} - \delta_a N_{0_a} = pNp \tag{3}$$

where

Y_{0_r} = acceleration sideways due to unit rudder deflection
L_{0_r} = rolling moment due to unit aileron deflection
N_{0_r} = yawing moment due to unit rudder deflection
N_{0_a} = yawing moment due to unit aileron deflection

The three unknowns in Eqs. (1), (2), and (3) are: r, δ_r, δ_a. Multiplying Eq. (1) by N_{0_r}/Y_{0_r}, and Eq. (2) by N_{0_a}/L_{0_a},

$$\delta_r = (-g/Y_{0_r}) \sin \Phi + (r/Y_{0_r})U_0 \tag{4}$$

$$\delta_a = \frac{1}{L_{0_a}}\frac{dp}{dt} - p\frac{1}{L_{0_a}}L_p - r\frac{1}{L_{0_a}}L_r \tag{5}$$

Substituting δ_r and δ_a in Eq. (3) and recalling that $\Phi = k\left(\frac{1 - e^{-nt}}{n} - \frac{1 - e^{-(n+m)t}}{n+m}\right)$,

$$\frac{dr}{dt} + Ar = C_1 e^{-nt} + C_2 e^{-(n+m)t} - g\frac{N_{0_r}}{Y_{0_r}} \sin \Phi \tag{6}$$

where

$$C_1 = N_p k - \frac{N_{0_a}}{L_{0_a}} kn - \frac{N_{0_a}}{L_{0_a}} L_p k$$

$$C_2 = -N_p k + \frac{N_{0_a}}{L_{0_a}} k(n+m) + \frac{N_{0_a}}{L_{0_a}} L_p k$$

$$A = \frac{N_{0_a}}{L_{0_a}} L_r - \frac{N_{0_r}}{Y_{0_r}} U_0 - N_r$$

Solving Eq. (6)

$$r = Be^{-At} + \frac{C_1}{A-n}\,e^{-nt} + \frac{C_2}{A-(n+m)}\,e^{-(n+m)t} - g\frac{N_{0_r}}{Y_{0_r}}\,e^{-At}\int_0^t e^{At}\sin\Phi\,dt$$

The boundary conditions are $r = 0$ at $t = 0$, therefore,

$$r = \frac{C_1}{A-n}\,(e^{-nt} - e^{-At}) + \frac{C_2}{A-(n+m)}\,(e^{-(n+m)t} - e^{-At}) - g\frac{N_{0_r}}{Y_{0_r}}\,e^{-At}\int_0^t e^{At}\sin\Phi\,dt \quad (7)$$

The integral term in this equation must be evaluated:

Let the true integral $= \int_0^t e^{Ax}\sin\Phi(x)\,dx$

Let the approximate integral $= \sin\Phi(t)\int_0^t e^{Ax}\,dx$

$$R = \text{true/approximate}$$

Integrating the approximate integral

$$R = \frac{A\int_0^t A(x-t)\sin\Phi(x)\,dx}{\sin\Phi(t)\,(1-e^{-At})}$$

For t small

$$\sin\Phi(t) = \Phi(t) + \frac{[\Phi(t)]^3}{3!} + \cdots\cdots$$

$\Phi(t)$ less than $1/2$

t less than $1/2$

For simplicity let,

$$I_1 = A\int_0^t e^{A(x-t)}\sin\Phi(x)\,dx = A\int_0^t e^{A(x-t)}\,\Phi(x)dx$$

Integrating by parts, recalling again that

$$\Phi(x) = k\left(\frac{1-e^{-nx}}{n} - \frac{1-e^{-(n+m)x}}{n+m}\right)$$

$$I_1 = \Phi(t) - k\left(\frac{e^{-nt}-e^{-At}}{A-n} - \frac{e^{-(n+m)t}-e^{-At}}{A-(n+m)}\right)$$

$$R = \frac{1 - \dfrac{k}{\Phi(t)}\left(\dfrac{e^{-nt}-e^{-At}}{A-n} - \dfrac{e^{-(n+m)t}-e^{-At}}{A-(n+m)}\right)}{1-e^{-At}} \quad (8)$$

Therefore, for values of t up to approximately $1/2$ sec.,

$$\int_0^t e^{At}\sin\Phi(t)\,dt = R\sin\Phi(t)\int_0^t e^{At}\,dt$$

where R is given in Eq. (8).

For t large

The integral can be evaluated by an asymptotic evaluation.

$$I_2 = e^{-Ax}\int_0^t e^{Ax}\sin\Phi(x)\,dx$$

Expressing $\sin\Phi(x)$ in a Taylor's series and substituting in the above integral

$$\sin\Phi(x) = \sin\Phi(t) + \cos\Phi(t)\,\frac{d\Phi}{dt}\,\frac{(x-t)}{1!} + \cdots.$$

$$\int_0^t e^{Ax}\sin\Phi(x)\,dx = \sin\Phi(t)\,\frac{e^{At}-1}{A} + \cos\Phi(t)\,\frac{d\Phi}{dt}\left[\frac{t}{A} - \frac{e^{At}-1}{A^2}\right]$$

Therefore

$$I_2 = \frac{\sin\Phi(t)}{A}\,(1-e^{-At})\times\left[1 - \left(\frac{\cot\Phi(t)}{A}\right)\left(\frac{d\Phi}{dt}\right)\left(\frac{1-e^{-At}-Ate^{-At}}{1-e^{-At}}\right)\right]$$

Summarizing

For t less than $1/2$ sec.,

$$e^{-At}\int_0^t e^{At}\sin\Phi(t)\,dt = R\,\frac{\sin\Phi(t)}{A}\,(1-e^{-At})$$

For t greater than $1/2$ sec.,

$$e^{-At}\int_0^t e^{At}\sin\Phi(t)\,dt = \frac{\sin\Phi(t)}{A}\,(1-e^{-At})\times\left[1 - \left(\frac{\cot\Phi(t)}{A}\right)\left(\frac{d\Phi}{dt}\right)\left(\frac{1-e^{-At}-Ate^{-At}}{1-e^{-At}}\right)\right]$$

Therefore, by solution of the lateral equations of motion through assuming a bank $\Phi(t)$ in a horizontal turn in which there is no sideslip, the rudder deflection, δ_r, the aileron deflection, δ_a, and the angular velocity of yaw, r, can be found in terms of the airplane accelerations for unit control movement, Y_{0_r}, L_{0_a}, N_{0_r}, N_{0_a} and damping derivatives L_r, L_p, N_p, N_r.

The Longitudinal Motions

The equations of motion in a longitudinal disturbance may be written,

$$du/dt = uX_u + wX_w - g\theta + X_0$$

$$dw/dt = uZ_u + wZ_w + qU_0 + Z_0$$

$$dq/dt = uM_u + wM_w + qM_q + M_0$$

As before, the quantities that arise in the consideration of the longitudinal motions are defined in *N.A.C.A. T.R. No. 560.*

Solution of the Longitudinal Equations

From the three longitudinal equations, the unknowns are: u, w, θ, X_0, Z_0, M_0.

As in the case concerning the lateral equations, there are three equations and six unknowns. One of the unknowns can be eliminated by letting $M_0 = \delta_e M_{0_e}$ and $Z_0 = \delta_e Z_{0_e}$.

For the other two unknowns: (1) $X_0 = 0$, i.e., no change in thrust; (2) $\theta = w/U_0$; and (3) steady state, i.e., $du/dt = 0$, $dw/dt = 0$.*

* Only the steady state condition of the turn will be considered, for that will determine maximum elevator deflection.

For some relation to give q (pitching velocity), consider the motion of the airplane as it executes a turn.

Using vector notation,

$$\bar{\omega} = p\bar{\imath} + q\bar{\jmath} + r\bar{k}$$

where $\bar{\omega}$ = angular velocity of coordinate.

If Ψ = change of direction in horizontal plane from original flight path (degree of turn executed), then,

$$\bar{\omega} = \frac{d\Phi}{dt}\bar{\imath} + \frac{d\Psi}{dt}\sin\Phi\bar{\jmath} + \frac{d\Psi}{dt}\cos\Phi\bar{k}$$

Therefore, $r = (d\Psi/dt)\cos\Phi$, $q = (d\Psi/dt)\sin\Phi$, and

$$d\Psi/dt = r\sec\Phi \tag{9}$$

Eliminating $d\Psi/dt$,

$$q = r\tan\Phi \tag{10}$$

Using assumptions 1, 2, and 3, and $q = r\tan\Phi$, the longitudinal equations may be written:

$$uX_u + wX_w - g(w/U_0) = 0$$

$$uZ_u + wZ_w + \delta_e Z_{0_e} = -U_0 q$$

$$uM_u + wM_w + \delta_e M_{0_e} = (D - M_q)q$$

$X_u = 0$*; therefore $w = 0$, and so

$$uZ_u + Z_{0_e}\delta_e = -U_0 q$$

$$uM_u + M_{0_e}\delta_e = (D - M_q)q$$

Solving for δ_e:

$$\delta_e = -(U_0 M_u q + Z_u(D - M_q)q)/(Z_{0_e}M_u - M_{0_e}Z_u) \tag{11}$$

Integrating Eq. (9) gives the turn as a function of time

$$\Psi = \int_0^t r\sec\Phi(t)dt \tag{12}$$

Knowing Ψ, the acceleration produced during the turn can easily be calculated.

Normal acceleration = $U_0\Omega$ ft./sec.^{2}, where, $\Omega = d\Psi/dt$.

Gravitational acceleration = 32.2 ft./sec.^{2} Therefore,

$$a = \sqrt{(a_n)^2 + (a_g)^2} \tag{13}$$

Calculations for Time to Execute a Steady Turn and the Control Deflections Necessary for a Typical Twin-Engined Attack Bomber

Dimensions and Characteristics of Airplane Considered

Wing area, S	= 465 sq.ft.
Wing span, b	= 61.33 ft.
Aspect ratio of wing, AR	= 8.09
Weight, W	= 19,300 lbs.
Taper ratio, σ	= 2.66:1
M.A.C., t	= 100.2 in.
Vertical surface area, S_V	= 63.28 sq.ft.
Aspect ratio of vertical surface, AR_V	= 1.38
Distance from c.g. to rudder hinge line, l_V	= 307.6 in.
Distance from c.g. to elevator hinge line, l_H	= 316.5 in.
Horizontal surface efficiency, η_H	= 0.60 (power on) = 0.72 (power off)
dC_{M_t}/dC_L	= −0.170 (power on) = −0.271 (power off)
Damping factor, K	= 5/4
Horizontal surface area, S_H	= 101 sq.ft.
Aspect ratio of horizontal surface, AR_H	= 4.50
K_x^2	= 49.2 ft.^{2}
K_y^2	= 59.8 ft.^{2}
K_z^2	= 104.1 ft.^{2}
C_{D_W}	= 0.035
U_0	= 280 m.p.h. (sea level) = 300 m.p.h. (15,000 ft.)
T_{C_0}'	= 0.0304 (sea level) = 0.0395 (15,000 ft.)
Propeller efficiency, η	= 0.87 (sea level) = 0.85 (15,000 ft.)

Resistance and Rotary Derivatives for Longitudinal Motions

$$X_u = -(2/mU_0)q'SC_D$$

$$Z_u = -(2/mU_0)q'SC_L$$

$$M_q = (q'S/mU_0)(K)(S_H/S)\left(\frac{l_H}{K_y}\right)^2\frac{a_0}{1 + (a_0/\pi AR_t)}\eta_H$$

The calculation of M_u presents some difficulty. If moment curves are available for various values of T_C' (Fig. 1), it is possible to get an approximate value of M_u.

It is known that $T_C'V^2 = T_{C_0}'V_0^2$ = const. or, rewriting, $V = V_0(T_{C_0}'/T_C')^{1/2}$, where $(\ )_0$ indicates equilibrium trim.

For power on, $T_{C_0}' = P\eta/q'SV_0$, where $P\eta$ = power available, q' = dynamic pressure, S = wing area, and V_0 = velocity for trim.

By interpolating a C_M vs. C_L curve for T_{C_0}' and shifting the C_L axis to intercept the curve at C_{L_0}, values of C_M' for various values of T_C' at trim C_L may be obtained. Since V is a function of T_C', it is therefore possible to plot various values of V for corresponding values of C_M',

$$uM_u = C_M'q'St(g/w)$$

$$M_u' = q'St(g/w)(C_M'/u)$$

$$M_u' = (1/C_{L_0})gt(dC_M'/dV)$$

* $X_u = 0$ and the assumption $X_0 = 0$ are not consistent except in the case for horizontal flight in a straight line at the speed U_0. The error produced by this inconsistency is small.

TABLE 1

STABILITY DERIVATIVES AND ACCELERATIONS FOR UNIT CONTROL MOVEMENT FOR TWIN-MOTORED ATTACK BOMBER

Altitude	X_u	Z_u	M_q	M_u	L_p	N_p	L_r	N_r	Y_{0_r}	Z_{0_e}	M_{0_e}	L_{0_a}	N_{0_r}	N_{0_a}
Sea level*	0	−0.151	−2.83	−0.00201	−7.00	−0.0694	0.326	−0.771	−0.579	−41.8	−0.467	0.771	0.1775	0.00443
15,000 ft.†	0	−0.109	−2.41	−0.00157	−4.71	−0.0468	0.221	−0.521	−0.420	−30.3	−0.339	0.559	0.1289	0.00325

* $C_- = 0.209$ } M_u based on change in C_M' at these constant values of C_L.
† $C_- = 0.287$ }

TABLE 2

TWIN-ENGINED AIRPLANE; SEA LEVEL CONDITIONS

t, sec.	Φ, rad.	r	r sec. Φ	Ψ, deg.	δ_r, deg.	δ_a, deg.	a_n, ft./sec.^{2}	a_s, ft./sec.^{2}	"g"
0	0	0	0	0	0	11.48	0	32.2	1.00
0.125	0.056	0.0039	0.0039	0.01	0.32	11.99	1.60	32.2	1.00
0.250	0.168	0.0122	0.0124	0.07	0.64	11.36	5.08	32.2	1.01
0.375	0.310	0.0229	0.0240	0.20	0.77	10.20	9.84	32.2	1.05
0.500	0.449	0.0330	0.0366	0.42	0.77	8.90	15.01	32.2	1.10
0.750	0.694	0.0493	0.0642	1.14	0.68	6.50	26.32	32.2	1.29
1.000	0.878	0.0596	0.0935	2.27	0.56	4.19	38.34	32.2	1.55
1.500	1.102	0.0695	0.1536	5.81	0.43	2.16	62.98	32.2	2.20
2.000	1.212	0.0730	0.2087	11.00	0.38	1.03	85.57	32.2	2.84
2.500	1.260	0.0743	0.2429	17.47	0.35	0.47	99.59	32.2	3.25
3.000	1.289	0.0750	0.2699	24.81	0.34	0.20	110.66	32.2	3.58
4.000	1.308	0.0754	0.2911	40.89	0.33	0.03	119.35	32.2	3.84
∞	1.313	0.0755	0.2960		0.33	−0.03	121.36	32.2	3.90

TABLE 3

TWIN-ENGINED AIRPLANE; 15,000-FT. CONDITIONS

t, sec.	Φ, rad.	r	r sec. Φ	Ψ, deg.	δ_r, deg.	δ_a, deg.	a_n, ft./sec.^{2}	a_s, ft./sec.^{2}	"g"
0	0	0	0	0	0	15.83	0	32.2	1.00
0.125	0.056	0.00376	0.0038	0.01	0.35	13.40	1.67	32.2	1.00
0.250	0.168	0.01152	0.0117	0.07	0.73	11.28	5.15	32.2	1.01
0.375	0.310	0.02147	0.0225	0.19	0.89	9.42	9.90	32.2	1.05
0.500	0.449	0.03093	0.0343	0.40	0.87	7.88	15.09	32.2	1.10
0.750	0.694	0.04613	0.0601	1.07	0.74	5.45	26.44	32.2	1.29
1.000	0.878	0.05572	0.0874	2.13	0.58	3.22	38.46	32.2	1.56
1.500	1.102	0.06488	0.1434	5.43	0.41	1.74	63.10	32.2	2.20
2.000	1.212	0.06818	0.1943	10.27	0.33	0.82	85.49	32.2	2.84
2.500	1.260	0.06938	0.2269	16.30	0.30	0.37	99.84	32.2	3.26
3.000	1.289	0.07005	0.2521	23.16	0.29	0.15	110.92	32.2	3.59
4.000	1.308	0.07042	0.2719	38.18	0.28	0.02	119.64	32.2	3.85
∞	1.313	0.07049	0.2765		0.29	−0.02	121.66	32.2	3.91

where dC_M'/dV may be obtained by taking the slope of the C_M' vs. V curve at V_0 (Fig. 2).

Dividing M_u' by K_y^2 gives the desired quantity, M_u.

Resistance Derivatives for Lateral Motion

$$L_p = \left(\frac{1}{\tau}\right)\left(\frac{1}{4}\right)\left(\frac{b}{K_x}\right)^2\left[\frac{dC_l}{d(pb/2V)}\right] \text{ (reference 3)}$$

$$(\tau = m/\rho SV)$$

$$N_p = \left(\frac{1}{\tau}\right)\left(\frac{1}{4}\right)\left(\frac{b}{K_z}\right)^2\left[\frac{dC_n}{d(pb/2V)}\right] \text{ (reference 3)}$$

$$L_r = \left(\frac{1}{\tau}\right)\left(\frac{1}{4}\right)\left(\frac{b}{K_x}\right)^2\left[\frac{dC_l}{d(pb/2V)}\right] \text{ (reference 3)}$$

$$N_r = \left(\frac{1}{\tau}\right)\left(\frac{1}{4}\right)\left(\frac{b}{K_z}\right)^2\left[\frac{d_nC}{d(pb/2V)}\right] \text{ (reference 3)}$$

where

$$\frac{dC_n}{d(rb/2V)} = -\frac{C_{DW}}{3} - 2\eta_V\left(\frac{l_V}{b}\right)^2\frac{S_V}{S}\frac{dC_{LV}}{d\beta} \text{ (reference 4)}$$

Accelerations for Unit Control Movement

$$Y_{0_r} = C_{Y_{0_r}}q'(S/m)$$
$$Z_{0_e} = C_{Z_{0_e}}q'(S/m)$$
$$M_{0_e} = C_{M_{0_e}}q'S(t/m)K_y^2$$
$$L_{0_a} = C_{l_{0_a}}q'S(b/m)K_x^2$$
$$N_{0_r} = C_{n_{0_r}}q'S(b/m)K_z^2$$
$$N_{0_a} = C_{n_{0_a}}q'S(b/m)K_z^2$$

Control Deflections and Transition Time Necessary for Airplane to Maneuver from Straight and Level Flight into a Steady Turn

An examination of the exponential curve

$$\Phi = k\left(\frac{1 - e^{-nt}}{n} - \frac{1 - e^{-(n+m)t}}{n + m}\right)$$

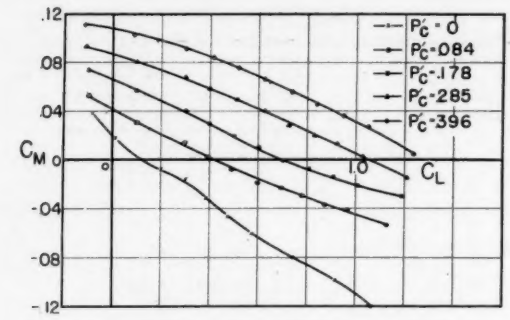

FIG. 1. Power on pitching moment coefficient curves.

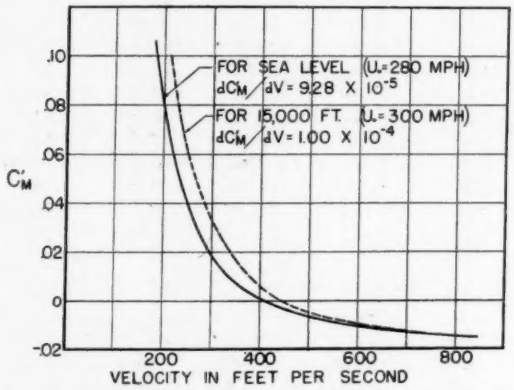

FIG. 2. Effect of power on pitching moment coefficient at trim lift coefficient. $C_{L_{trim}} = 0.209$ at sea level and 0.287 at 15,000 ft.

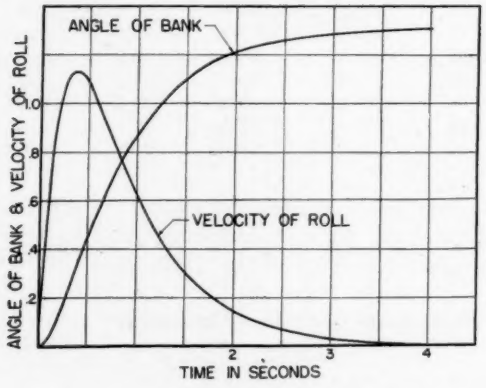

FIG. 3. Assumed velocity of roll and angle of bank.

will reveal that the parameter, k, determines the maximum angle of bank, whereas the other two parameters, n and m, determine the rolling velocity and, therefore, the helix angle $pb/2V$.

For a maximum bank of 75° and a helix angle of approximately 0.090, the parameters should be $k = 2.95$, $m = 3.0$, and $n = 1.5$.

Using the values of the stability derivatives and accelerations for unit control deflection for sea level (see Table 1), $A = 126.5$, $C_1 = -0.1102$, and $C_2 = 0.1618$.

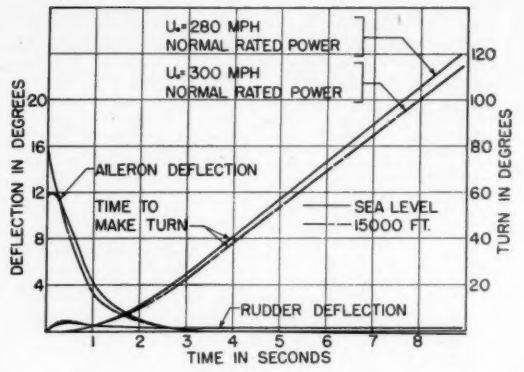

FIG. 4. Time to turn and necessary control deflections for twin-engined airplane.

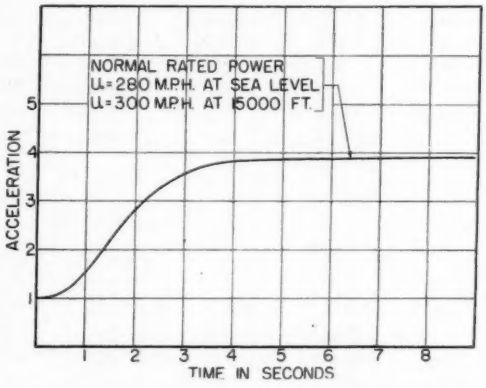

FIG. 5. Acceleration during turn for twin-engined airplane and single-engined airplane.

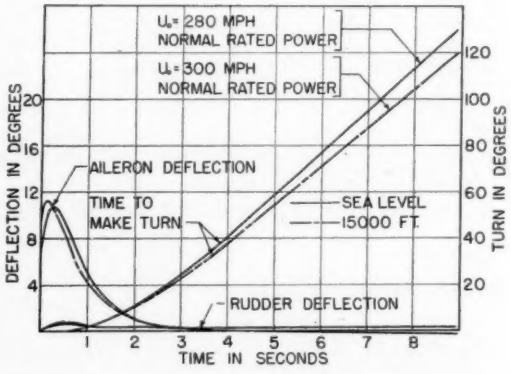

FIG. 6. Time to turn and necessary control deflections for single-engined airplane.

By assuming various values of t and graphically integrating Eq. (12), the time to enter into steady turning flight can be obtained. Substitution of the proper values into Eqs. (4) and (5) gives control deflections, δ_r and δ_a, necessary to execute this maneuver. Since $d\Psi/dt$ is known from Eq. (9), the acceleration produced can be readily calculated (Table 2).

Fig. 3 shows Φ and p plotted against time t, while

TABLE 4

STABILITY DERIVATIVES AND ACCELERATIONS FOR UNIT CONTROL MOVEMENT FOR MODIFIED SINGLE-ENGINED AIRPLANE

Altitude	X_u	Z_u	M_q	M_u	L_p	N_p	L_r	N_r	$Y_{\delta r}$	$Z_{\delta e}$	$M_{\delta e}$	$L_{\delta a}$	$N_{\delta r}$	$N_{\delta a}$
Sea level*	0	−0.151	−2.83	−0.00201	−12.37	−0.0779	0.576	−0.865	−0.579	−41.8	−0.467	1.360	0.1994	0.00669
15,000 ft.†	0	−0.109	−2.41	−0.00157	− 8.33	−0.0675	0.391	−0.585	−0.420	−30.3	−0.339	0.986	0.1447	0.00490

* $C_L = 0.209$ } M_u based on change in $C_{M'}$ at these constant values of C_L.
† $C_L = 0.287$ }

Fig. 4 shows the time to turn along with the necessary aileron and rudder deflections. The acceleration produced during the maneuver is shown in Fig. 5.

Eq. (11) gives δ_e necessary to hold steady turning flight. Since $q = r \tan \Phi$, $\delta_{e_{max.}}$ can be obtained by using a large value of time, t. For this particular case, $\delta_e = -8.4°$.

Considering the same values of k, m, and n and using the proper stability derivatives and accelerations for unit control deflection for 15,000 ft., the time to enter into a steady turn and the control deflections necessary can be calculated (see Table 3).

Fig. 4 shows (dashed lines) the time to turn along with the necessary aileron and rudder deflections, and Fig. 5 shows the acceleration produced during the turn.

$\delta_e = -10.5°$ in the steady state turn.

From an examination of Fig. 4 it is apparent that there is little difference in the time required to make a specified turn assuming ample aileron control. As would be expected, however, the control deflections must be considerably increased for the high-altitude case, which might make it impossible for the pilot to obtain the same rolling velocity at the two altitudes, meaning a loss in maneuverability as the airplane ascends.

The elevator deflection necessary to hold steady turning flight is slightly increased due to altitude, but the acceleration produced remains unchanged.

The maneuvering characteristics investigated have been for a twin-motored attack bomber of late design. By assuming a modified single-engined airplane with one motor mounted in the fuselage and of the same weight and total horsepower as the two motors on the twin-engined airplane, the aerodynamic qualities necessary for the calculations remain unchanged. Only the radii of gyration come in as influencing factors. Therefore it should be of interest to investigate the maneuvering qualities of an aerodynamically similar airplane, but one with different mass distribution.

Assume that the top speed remains unchanged and the single motor is mounted 6 ft. forward of the two motors on the previously discussed airplane.

The known quantities are:

(1) Radii of gyration of twin-motored airplane: $K_x^2 = 49.2$ ft.^{2}, $K_y^2 = 59.8$ ft.^{2}, and $K_z^2 = 104.1$ ft.^{2}

(2) Weight of engine on twin-motored airplane: $W = 2690$ lbs.

(3) Weight of engine on single-motored airplane: $2W = 5380$ lbs.

(4) Distance of motor from fuselage on twin-motored airplane: $y = 8.75$ ft.

(5) Distance motor moved forward on single-motored airplane: $x = 6.00$ ft.

By denoting I_S and I_T as moment of inertia of single- and twin-motored airplane, respectively: I_S = mass of airplane $\times K_X^2$ − inertia due to motors.

Therefore,

$$K_X^2 = I_S/\text{mass of airplane}$$

In a similar manner K_y^2 and K_z^2 can be approximated for the single-engined airplane.

The new values for radii of gyration are: $K_x^2 = 27.9$ ft.^{2}, $K_y^2 = 69.8$ ft.^{2}, and $K_z^2 = 92.9$ ft.^{2}

Using these new radii of gyration, the stability derivatives and accelerations for unit control deflection can be calculated (see Table 4).

Again considering the same values of k, m, and n and using the proper stability derivatives and accelerations from Table 4, the time to maneuver into steady turning flight and the control deflections necessary can be calculated. Fig. 6 shows the time to turn and the necessary aileron and rudder deflections for sea level and 15,000 ft. Fig. 5 shows the acceleration produced.

$\delta_e = -8.4°$ at sea level in the steady state turn.
$\delta_e = -10.5°$ at 15,000 ft. in the steady state turn.

It is of interest to note that for this "new" airplane consisting of one engine the time to execute a given turn remains substantially the same as that required for the original twin-engined one. The initial aileron deflection at sea level for this single-engined airplane is fairly low, but from Fig. 6 it is seen that the aileron position must reach in short time almost that required for the first airplane considered. However, at 15,000 ft. the initial aileron deflection is increased only a few degrees and reaches a maximum value after a *finite* time period, which differs from the aileron position-time curve for the twin-engined airplane, which shows a maximum deflection at zero time. For this modified airplane the maximum aileron position necessary at 15,000 ft. is only a fraction of one degree greater than that necessary at sea level, whereas, for the twin-engined airplane, the altitude case required over 4° additional deflection.

The elevator positions are the same for both airplanes at a given altitude and accelerations unchanged with regard to altitude and configuration.

The rudder deflections required are small for all cases.

TABLE 5

MODIFIED SINGLE-ENGINED AIRPLANE; SEA LEVEL CONDITIONS

t, sec.	Φ, rad.	r	$r \sec \Phi$	Ψ, deg.	δ_r, deg.	δ_a, deg.	a_n, ft./sec.^{2}	a_g, ft./sec.^{2}	"g"
0	0	0	0	0	0	6.50	0	32.2	1.00
0.125	0.056	0.00402	0.0040	0.01	0.26	9.81	1.64	32.2	1.00
0.250	0.168	0.01237	0.0125	0.07	0.52	10.66	5.13	32.2	1.01
0.375	0.310	0.02306	0.0242	0.21	0.63	10.25	9.92	32.2	1.05
0.500	0.449	0.03319	0.0368	0.42	0.63	9.34	15.09	32.2	1.10
0.750	0.694	0.04945	0.0644	1.15	0.57	7.06	26.40	32.2	1.29
1.000	0.878	0.05970	0.0936	2.29	0.49	4.83	38.38	32.2	1.56
1.500	1.102	0.06950	0.1537	5.83	0.39	2.42	63.02	32.2	2.20
2.000	1.212	0.07301	0.2081	11.01	0.35	1.15	85.32	32.2	2.83
2.500	1.260	0.07429	0.2430	17.48	0.33	0.52	99.63	32.2	3.25
3.000	1.289	0.07499	0.2699	24.82	0.34	0.22	110.66	32.2	3.58
4.000	1.308	0.07541	0.2912	40.90	0.32	0.03	119.39	32.2	3.84
∞	1.313	0.07549	0.2961		0.32	−0.03	121.40	32.2	3.90

TABLE 6

MODIFIED SINGLE-ENGINED AIRPLANE; 15,000-FT. CONDITIONS

t, sec.	Φ rad.	r	$r \sec \Phi$	Ψ, deg.	δ_r, deg.	δ_a, deg.	a_n ft./sec.^{2}	a_g, ft./sec.^{2}	"g"
0	0	0	0	0	0	8.95	0	32.2	1.00
0.125	0.056	0.00380	0.00380	0.01	0.30	11.38	1.67	32.2	1.00
0.250	0.168	0.01163	0.01179	0.07	0.61	10.30	5.19	32.2	1.01
0.375	0.310	0.02162	0.02270	0.19	0.73	9.48	9.99	32.2	1.05
0.500	0.449	0.03107	0.03449	0.40	0.72	8.43	15.16	32.2	1.11
0.750	0.694	0.04624	0.06020	1.08	0.62	6.22	26.49	32.2	1.30
1.000	0.878	0.05580	0.08749	2.14	0.50	4.10	38.50	32.2	1.87
1.500	1.102	0.06493	0.14356	5.45	0.36	2.09	63.17	32.2	2.20
2.000	1.212	0.06819	0.19434	10.29	0.32	0.99	85.51	32.2	2.84
2.500	1.260	0.06939	0.22697	16.32	0.29	0.45	99.87	32.2	3.26
3.000	1.289	0.07005	0.25211	23.19	0.29	0.19	110.93	32.2	3.59
4.000	1.308	0.07042	0.27189	38.20	0.29	0.02	119.63	32.2	3.85
∞	1.313	0.07049	0.27646		0.28	−0.02	121.64	32.2	3.91

CONCLUSION

The effect of altitude (15,000 ft.) on the maneuvering characteristics of a twin-motored airplane is apparent. There appears to be little difference in the time to make a specified turn, but the aileron deflection must be considerably increased for the high-altitude case.

At sea level, the investigation of the maneuvering characteristics of the single-engined airplane—i.e., the twin-engined airplane considered to be powered by a single engine but otherwise unchanged—showed that for this modified condition the time to make a given turn and the rudder and aileron deflections necessary to execute this maneuver differed little from that required for the original twin-engined airplane. The initial aileron deflection required for the modified airplane is less than that necessary for the twin-engined one but quickly builds up to nearly the same maximum. Therefore, at sea level it appears that there is little difference in the maneuverability of the two airplanes.

The effect of altitude on the single-engined airplane is slight. The initial aileron deflection increases, but the maximum deflection required remains the same. The rudder deflections and time to make a specified turn are only slightly changed. Since altitude has such a small effect on this modified single-engined airplane, it certainly should be superior in maneuvering qualities to the twin-engined one.

Accelerations remain the same for all cases considered.

REFERENCES

[1] Dickinson, H. B., *Maneuverability and Control Surface Strength Criteria for Large Airplanes*, Journal of the Aeronautical Sciences, Vol. 7, p. 469, September, 1940.

[2] Jones, Robert T., *A Simplified Application of the Method of Operators to the Calculation of Disturbed Motions of an Airplane*, N.A.C.A. T.R. No. 560, 1936.

[3] Pearson, Henry A., and Jones, Robert T., *Theoretical Stability and Control Characteristics of Wings with Various Amounts of Taper and Twist*, N.A.C.A. T.R. No. 635, 1938.

[4] Millikan, Clark B., *Aerodynamics of the Airplane* John Wiley & Sons, New York, 1941.

Fatigue Characteristics of Natural and Resin-Impregnated, Compressed, Laminated Woods

FORREST B. FULLER* AND TURE T. OBERG†
Wright Field

SUMMARY

Because of the increased demand for the production of aircraft, natural woods are being used for primary structural members and propeller blades are being fabricated from both natural and resin-impregnated, compressed, laminated hard woods. Although there are considerable data available on the static properties of wood, information about action under repeated stresses is quite limited.[1-8] Therefore, fatigue properties have been determined for natural and compressed woods on specimens with and without notches. The rotating beam fatigue machine, which employs a constant load and has been satisfactorily used for testing metals, was also found suitable for testing wood. Tests were run to 100,000,000 reversals or cycles, at relatively low and high frequencies, a few being continued to 500,000,000 cycles. Relatively low notch sensitivity was found for the natural and compressed woods. The ratio of the fatigue limit in bending to the modulus of rupture in static bending was about 0.2 for circular or round sections.

MATERIALS

NATURAL HARD MAPLE and yellow birch woods of aircraft grade with straight grain, as well as non-impregnated and resin-impregnated, compressed, laminated hard maple and yellow birch of commercial processing, were tested. A description of the materials, including specific gravity and moisture content, is given in Table 1. The values for moisture content for the compressed, resin-impregnated woods are in reality percentage loss of weight rather than moisture content. The impregnating and bonding materials were thermo-setting phenol-formaldehyde resins of the paper film and liquid types. Laminated, as used herein, refers to that type of construction in which the laminations or veneers (thin pieces of wood) are bonded together with the grain in all laminations parallel as contrasted with plywood in which the grain in alternate laminations is parallel but perpendicular to that in adjacent laminations.

TABLE 1
Description of Material

Test No.	Moisture Content, Per Cent	Specific Gravity	Species	Description
1	8.0	0.70	Hard maple	Natural wood—solid (nonlaminated)
2	3.3	0.68	Hard maple	Natural wood, 1/8 in. laminations, noncompressed, nonimpregnated, phenolic resin paper bonding
3	3.5	1.23	Hard maple	Compressed wood, 1/8 in. laminations, 50 per cent, impregnated, phenolic resin content, 12 per cent
4	3.1	1.31	Hard maple	Compressed wood, 1/8 in. laminations, 50 per cent, impregnated, phenolic resin content, 23 per cent
5	1.6	1.38	Hard maple	Compressed wood, 1/8 in. laminations, 50 per cent, phenolic resin paper bonding, nonimpregnated
6	7.0	0.69	Yellow birch	Natural wood—solid (nonlaminated)
7	1.7	1.25	Yellow birch	Compressed wood, 1/16 in. laminations, approximately 35 per cent, impregnated, phenolic resin content, 35 per cent
8*	3.1	1.36	Hard maple	Compressed wood, 1/8 in. laminations, 50 per cent, impregnated, phenolic resin content, 23 per cent
9	4.4	1.12	Yellow birch	Compressed wood, 1/8 in. laminations, nonimpregnated, phenolic resin bonding

* This specimen was the large type having 1 in. diameter in the gauge.

TEST PROCEDURE

Static Tests

Tensile, compressive and bend specimens were prepared and tested in accordance with procedures that are now incorporated in Federal Specification L-P-406.[9] The bend specimens were rectangular in cross section with a span approximately 16 times the depth. All specimens were tested under comparable laboratory conditions of temperature and humidity and with the stresses occurring parallel to the grain of the wood. Moisture content and specific gravity were determined in accordance with standard practice for wood as specified in Army-Navy aeronautical specifications on the oven dry weight and volume basis.[10]

Endurance or Fatigue Tests

Tests were made on ball-bearing rotating-beam fatigue machines, similar to the R. R. Moore type, Fig. 1. In this machine the specimen is a rotating beam of circular cross section supported at the ends and loaded with two symmetric loads producing a constant bending moment between the loads. The specimen is rotated under load, the stresses alternating equally between tension and compression. The unit stress in the extreme fiber of the specimen is computed by the standard bending formula $S = MC/I$, where

Received February 3, 1943.

* Major, Air Corps, Army Air Forces Matériel Center.
† Aeronautical Materials Testing Engineer, Army Air Forces Matériel Center.

FIG. 1. Rotating beam fatigue testing machine—wood specimen in place.

S = modulus of rupture or the unit stress in the extreme fiber in compression or tension, lbs. per sq.in.
M = bending moment of the section, in.-lbs.
I = moment of inertia of the cross section, in.^{4}
C = distance from the neutral axis to the extreme fiber or the radius at mid-span, in.

The type of specimens, the type of surface finishing and the testing were also in accordance with procedures that are now incorporated in Federal Specification L-P-406. Tests were made at frequencies of 3,450 and 10,600 r.p.m. on notched and unnotched specimens of the short type, Fig. 2. Stresses for notched specimens were based on the root section of the notch. The length of the specimens was parallel to the grain of the wood. The reduced section of each specimen after turning in a lathe was finished successively with sandpaper and Nos. 1, 0 and 00 emery paper.

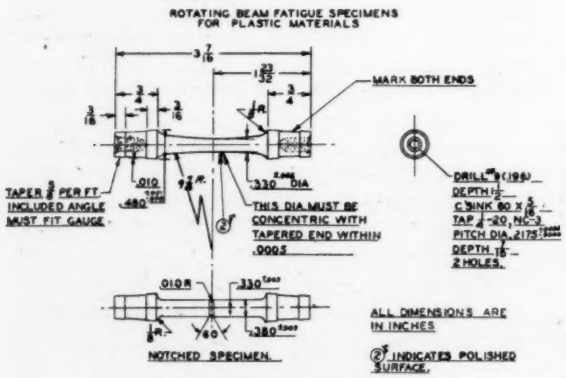
ROTATING BEAM FATIGUE SPECIMENS FOR PLASTIC MATERIALS
MARK BOTH ENDS
TAPER PER FT INCLUDED ANGLE MUST FIT GAUGE
THIS DIA MUST BE CONCENTRIC WITH TAPERED END WITHIN .0005
DRILL DEPTH C'SINK 80 X TAP -20, NC-3 PITCH DIA. DEPTH TO 2 HOLES.
ALL DIMENSIONS ARE IN INCHES
INDICATES POLISHED SURFACE.
NOTCHED SPECIMEN

FIG. 2.

The tests were conducted in a room in which the temperature and humidity conditions did not fluctuate appreciably. The weight of the specimens after testing was not determined, but it is believed that no serious change in moisture content occurred during the tests.

Impact data were obtained on $^1/_2$-in. square specimens of the standard notched Izod type with the notch transverse to the grain and parallel to the face of the laminations. The specimens were tested in an Olsen plastics impact tester of 100-in.lb. capacity.

RESULTS

The mechanical properties of the various woods are given in Table 2. The data are incomplete for some of the woods because of the lack of sufficient material.

The fatigue or endurance limit is that stress to which a material may be subjected for an indefinite number of reversals without failure. While the fatigue limit for steels in general is obtained at 10,000,000 stress cycles, it has been found that a larger number is necessary for aluminum alloy. In an investigation on the fatigue strength of natural walnut, ash, pine and spruce in the rotating-beam type fatigue machine, the knee on the S-N (stress-number of cycles) curves was reported between 20,000 and 2,000,000 stress reversals—that is, an endurance or fatigue limit was determined between 20,000 and 2,000,000 stress reversals.[4]

TABLE 2

Average Static Mechanical Properties Parallel to the Grain

Test No.	Izod Impact, Ft.Lbs. per In. of Notch	Ultimate Tensile Strength, Lbs. per Sq.In.	Ultimate Compressive Strength, Lbs. per Sq.In.	Bending Modulus of Rupture, Lbs. per Sq.In.
1			9,700	19,600
2			14,200	19,000
3	7.7	30,000	24,000	41,000
4	6.0	33,000	27,000	41,000
5				41,000
6			11,200	21,700
7	3.11	31,300		31,000
8	8.6	25,000	25,600	32,300
9			24,400	48,200

Fatigue data for the natural and compressed woods are given in Table 3 and shown in Fig. 3. The data on the S-N curve for resin impregnated, compressed, laminated yellow birch indicate that the actual fatigue limit was not obtained at 500,000,000 stress cycles, one specimen failing in the fatigue machine at 435,000,000 cycles at a stress of 10,000 lbs. per sq.in. The tests on the specimens for this particular material were stopped at 500,000,000 stress cycles, although this was not sufficient to reach the knee on the S-N curve. Retests were made on these specimens by increasing the stress without stopping the machine and the specimens run to failure. The number of cycles for each retest was compared with that for the specimen tested initially at the same stress. If this value for the retested specimens was lower than that for the original or initial test, the material was probably injured during the initial stressing. Only the original data are plotted on the S-N curve, Fig. 3, the values for the retest being given in Table 4.

For unnotched material, the fatigue limit for natural hard maple wood was determined at 4,000 lbs. per sq.in.

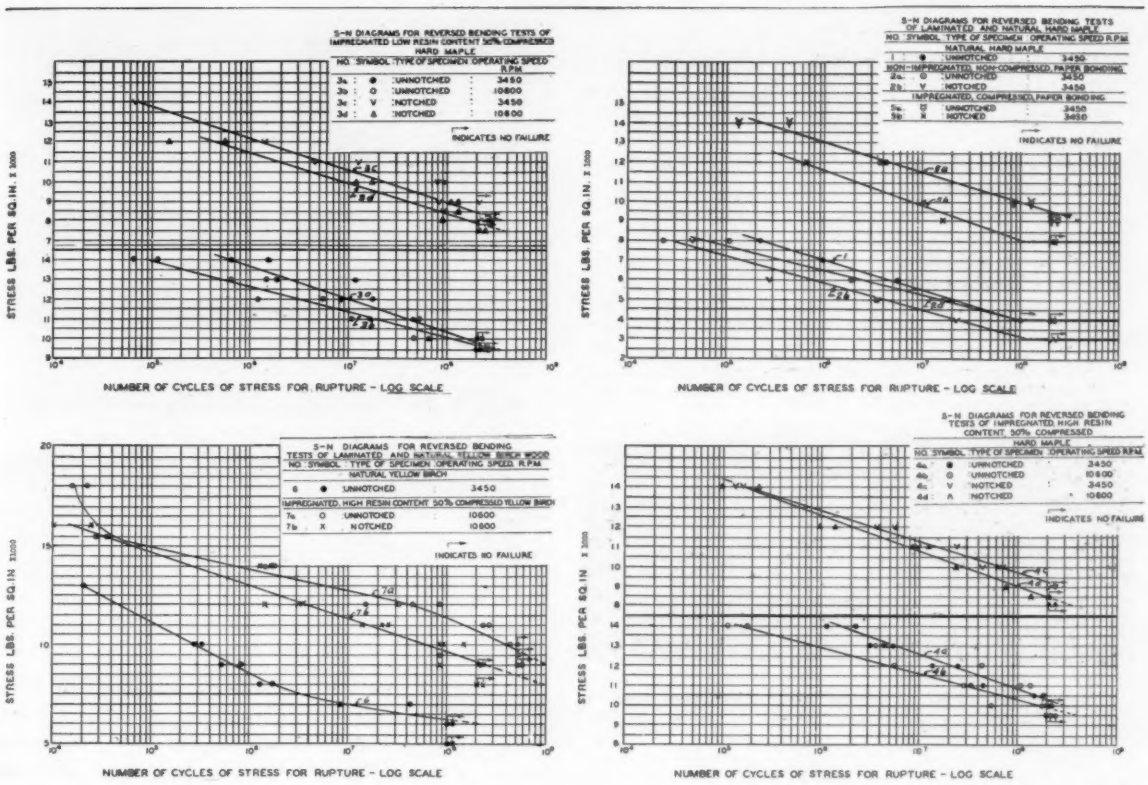
S-N DIAGRAMS FOR REVERSED BENDING TESTS OF IMPREGNATED LOW RESIN CONTENT 30% COMPRESSED HARD MAPLE
NO. SYMBOL TYPE OF SPECIMEN OPERATING SPEED R.P.M.
3a UNNOTCHED 3450
3b UNNOTCHED 10800
3c NOTCHED 3450
3d NOTCHED 10800
INDICATES NO FAILURE
STRESS LBS. PER SQ. IN. X 1000
NUMBER OF CYCLES OF STRESS FOR RUPTURE - LOG SCALE
S-N DIAGRAMS FOR REVERSED BENDING TESTS OF LAMINATED AND NATURAL HARD MAPLE
NO. SYMBOL TYPE OF SPECIMEN OPERATING SPEED R.P.M.
NATURAL HARD MAPLE
UNNOTCHED 3450
NON-IMPREGNATED, NON-COMPRESSED, PAPER BONDING
2a UNNOTCHED 3450
2b NOTCHED 3450
IMPREGNATED, COMPRESSED, PAPER BONDING
5a UNNOTCHED 3450
5b NOTCHED 3450
INDICATES NO FAILURE
STRESS LBS. PER SQ. IN. X 1000
NUMBER OF CYCLES OF STRESS FOR RUPTURE - LOG SCALE
S-N DIAGRAMS FOR REVERSED BENDING TESTS OF LAMINATED AND NATURAL YELLOW BIRCH WOOD
NO. SYMBOL TYPE OF SPECIMEN OPERATING SPEED R.P.M.
NATURAL YELLOW BIRCH
6 UNNOTCHED 3450
IMPREGNATED, HIGH RESIN CONTENT 50% COMPRESSED YELLOW BIRCH
7a UNNOTCHED 10800
7b NOTCHED 10800
INDICATES NO FAILURE
STRESS LBS. PER SQ. IN. X 1000
NUMBER OF CYCLES OF STRESS FOR RUPTURE - LOG SCALE
S-N DIAGRAMS FOR REVERSED BENDING TESTS OF IMPREGNATED, HIGH RESIN CONTENT, 50% COMPRESSED HARD MAPLE
NO. SYMBOL TYPE OF SPECIMEN OPERATING SPEED R.P.M.
4a UNNOTCHED 3450
4b UNNOTCHED 10800
4c NOTCHED 3450
4d NOTCHED 10800
INDICATES NO FAILURE
STRESS LBS. PER SQ. IN. X 1000
NUMBER OF CYCLES OF STRESS FOR RUPTURE - LOG SCALE

FIG. 3.

TABLE 3

Comparison of Endurance Limit with Static Properties

Test No.	Endurance Limit, Rotating Beam, Lbs. per Sq.In. — Unnotched specimen operating speed, r.p.m. — 3,450	10,600	Notched specimen operating speed, r.p.m. — 3,450	10,600	Ratio of Endurance Limit of Unnotched Material to Average Ultimate Static Properties — Tension	Compression	Bending — Rectangular cross section	Bending — Circular cross section
1	4,000*					0.412	0.204	0.173
2	4,000*		3,000*			0.282	0.210	0.178
3	9,500†	9,500†	8,000†	7,500†	0.316	0.396	0.232	0.197
4	10,000†	9,500†	9,000†	8,000†	0.288	0.352	0.232	0.197
5	9,500†		8,000†				0.232	0.197
6	6,000*					0.536	0.276	0.234
7		9,000‡	9,000‡	8,000‡	0.287		0.290	0.246
8	7,500**				0.300	0.293	0.232	0.197
9	10,000*	9,000*				0.410	0.207	0.176

* Endurance limit based on 100,000,000 cycles.
† Endurance limit based on 200,000,000 cycles.
‡ Endurance limit based on 500,000,000 cycles.
** Endurance limit based on 100,000,000 cycles and 1200 r.p.m.

and for natural yellow birch at 6,000 lbs. per sq.in., although the moisture content and specific gravity were about the same. The values for the compressed woods were higher with correspondingly higher specific gravity. No appreciable variation in fatigue strength was found between compressed maple containing 23 and 12 per cent phenolic resin. In the high-resin material, longitudinal cracks in the lamination were noted in both the unnotched and notched specimens after 200,000,000 stress cycles, Fig. 4. The characteristics or appearances of the fracture in the natural and compressed woods are different from those of metals. In general, they are irregular and jagged throughout the cross section, Figs. 6 and 8, whereas in metals

TABLE 4

Fatigue Values of Impregnated, Compressed Yellow Birch Wood —Unnotched Specimens

Original Tests		Retests	
Stress, lbs. per sq.in.	Number of cycles	Stress, lbs. per sq.in.	Number of cycles
12,000	45,000,000 F*		
12,000	91,100,000 F*		
12,000	32,000,000 F*		
12,000	15,200,000 F*		
10,000	500,100,000	12,000	8,889,000 F*
9,500	515,200,000	12,000	10,600,000 F*
9,000	500,350,000	12,000	15,600,100 F*

* F denotes failure of the specimen in the fatigue machine.

FIG. 4. Note cracks in lamination in compressed, impregnated, phenol-formaldehyde, high-resin content, laminated, hard maple, notched fatigue specimen.

there is a smooth surface due to the closing and opening of the crack during the cyclic stressing, followed by a rather small irregular area occurring at the time of complete failure.

For notched material, the fatigue limits were somewhat lower. However, the impregnated, compressed, laminated maple and birch are low in notch sensitivity, being relatively insensitive to the effect of notches under repeated bending stresses. No data of this type were obtained on natural wood. Notch sensitivity is the ratio of the fatigue limit of a notched specimen to that of an unnotched specimen. The variation in fatigue strength with increase in the resin content from 12 to 23 per cent for the compressed maple for notched specimens was negligible as noted in Table 3. The notched impregnated, compressed, laminated yellow birch failed in shear under repeated bending stresses. This type of failure is shown in natural size in Fig. 5 and in an enlarged view in Fig. 6. The failures of the other materials are in general normal.

The results given in Table 3 and Fig. 3 indicate no appreciable difference in the fatigue limits at a frequency of 3,450 and 10,600 r.p.m. for impregnated, compressed, laminated wood. No data were obtained on natural wood. However, the sloping part of the curves in the S-N diagrams, Fig. 3, which represents actual failure of specimens in the fatigue machine, indicates that the materials have lower fatigue resistance at stresses above the fatigue limit at the higher frequency.

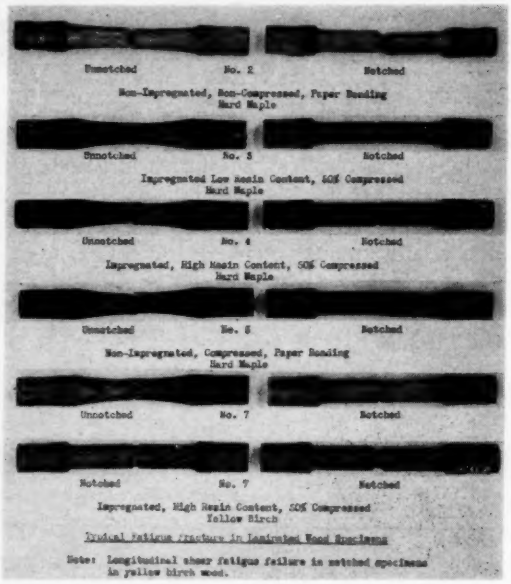

FIG. 5.

In metallic materials a definite relation has been found between the fatigue limit in bending and the static ultimate tensile strength. This ratio for ferrous metals varies from 0.44 to 0.55 and for nonferrous metals from 0.22 to 0.45. For woods, the ratios of the bending endurance limit on round specimens to static tensile, compressive and bend data are given in Table 3. The static bend data that were obtained on rectangular specimens have been corrected for circular sections by a form factor.[5] The ratios, based on tensile and compressive data, are quite erratic, but those for the bending are more uniform. The natural and impregnated, compressed birch had higher ratios than maple.

A series of fatigue tests at 1,200 r.p.m. was also made on large specimens, identified as Test No. 8, approximately 1 in. in diameter in the gauge section compared to the small specimens from compressed, impregnated hard maple with 23 per cent resin content. The material was similar in construction and fabrication to that used for the small specimens. The machine, comparable in principle to the small R. R. Moore machine,

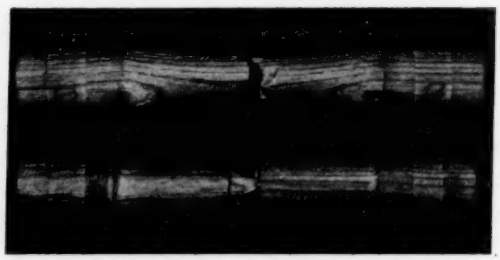

FIG. 6. View of fatigue failures in compressed, impregnated, phenol-formaldehyde high-resin content, laminated yellow birch, jagged in the unnotched and shear in the notched specimen.

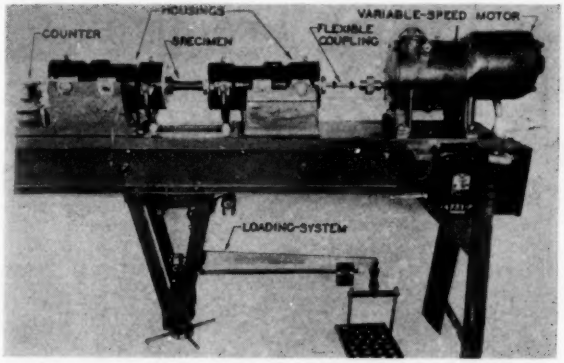

FIG. 7. Rotating beam fatigue testing machine. Capacity—approximately 2,000 lbs.

FIG. 8. Rotating beam fatigue failure. Large specimen. Compressed, impregnated hard maple with resin content of 23 per cent.

Fig. 7, was of larger capacity throughout, could be loaded either direct or by a lever system, and was driven by a variable speed motor of 600 to 2,100 r.p.m. Although the fatigue limit was lower than that for small specimens, the mechanical properties were also lower. However, it is of interest to note that the ratios of fatigue limit to static bending were comparable, Test No. 4 and No. 8, Table 3. A typical failure is shown in Fig. 8. The fatigue limit using five specimens was determined at 100,000,000 cycles, two specimens being stressed at 7,500 lbs. per sq.in. without failure and one at 8,000, one at 10,000, and one at 12,000 lbs. per sq. in. with failures, Table 5. Sufficient tests have not as yet been made to obtain a complete fatigue curve; however, the data for the five tests are indicative

TABLE 5

Fatigue Values of Impregnated, Compressed Hard Maple Wood—Large Unnotched Specimens (See Fig. 8)

Original Tests	
Stress, lbs. per sq.in.	Number of cycles
12,000	3,201,000 F*
10,000	4,450,000 F*
8,000	82,500,000 F*
7,500	101,000,000
7,500	105,000,000

* F denotes failure of the specimen in the fatigue machine.

REFERENCES

[1] Angstrom Tord-K, *Aeronautical Research in Sweden [on Wood]*, Journal of the Royal Aeronautical Society, Vol. 33, No. 226, pp. 897–914, October, 1929.

[2] Stanton, T. E., *Resistance of Wood to Stress Reversals*, Engineering (London), June 16, 1916.

[3] Moore, H. F., and Kommers, J. B., *The Fatigue of Metals*, 1929, Chap. X, pp. 244–249, 1929.

[4] Kraemer, Otto, *Bending Fatigue Tests on Wood*, Luftfahrtforschung, Vol. 8, No. 2, p. 39, July 15, 1930.

[5] Markwardt, L. J., and Wilson, T. R., *Strength and Related Properties of Woods Grown in the United States*, Technical Bulletin No. 479, U.S. Department of Agriculture, pp. 59–61, September, 1935.

[6] Kraemer, Otto, *Synthetic Resins and Their Development for Aircraft Construction*, Zeitschrift für Flugtechnik and Motorluftschiffahrt, Vol. 24, pp. 420–426, 1933.

[7] Dietz, G. H., and Grinsfelder, Henry, *Behavior of Plywood under Repeated Stresses*, Preprint of paper presented at the Woodworking Industries Meeting of the American Society of Mechanical Engineers, October 12, 1942.

[8] Oberg, T. T., Schwartz, R. T., and Shinn, D. A., *Mechanical Properties of Plastics at Normal and Subnormal Temperatures*, Air Corps Technical Report No. 4648, War Department, Army Air Forces Matériel Center, Wright Field, Dayton, O., June 6, 1941.

[9] Federal Specification L-P-406: General Specification (Methods of Test) for Organic Plastics.

[10] Army-Navy Aeronautical Specifications: AN-W-3, *Determination of Moisture Content of Wood*, April 24, 1942; AN-W-4a, *Determination of Specific Gravity of Wood*, April 24, 1942.

Effect of Cold-Work and Heat-Treatment on 24ST Aluminum Alloy

BRUCE MITCHELL*

Consolidated Aircraft Corporation

Introduction

The compressive yield strength of 24ST aluminum alloy extrusions is listed in the ANC-5 as 38,000 lbs. per sq.in. This value, generally used for design, is the guaranteed minimum for this material, but the actual yield strength of some specimens may run as high as 56,000 lbs. per sq.in. Thus 18,000 lbs. per sq.in. additional strength is lost to the designer because his "weakest link" has a yield strength of 38,000 lbs. per sq.in.

Aircraft engineers have been testing and studying this material for some time in an endeavor to utilize this possible increase in strength. The growing list of papers published on this subject indicates some gain in cold-working for additional strength, an increased knowledge of this alloy in the plastic region, and some attempts at predicting the compressive yield from the tensile strength of test specimens.

All of the data used in the preparation of this paper were obtained from tests made in the laboratory of Consolidated Aircraft Corporation. From these data, a more accurate method of calculating the compressive yield from the tensile properties will be developed and, it is hoped, some additional light will be thrown on the general characteristics of 24ST aluminum alloy.

Description of Tests

During the course of this investigation at Consolidated more than a hundred tests were made on 54 different hat-type stringers under a number of different conditions of heat-treatment and cold-work. Forty of these were extruded hats $1^1/_2$ in. deep with a nominal gauge of 0.078 in. The remaining 14 were rolled hats $1^1/_2$ in. deep made from 24ST Alclad sheet. The Alclad hats were made from standard sheets in gauges ranging from 0.072 to 0.128 in. Sections of the hats $5^1/_4$ in. long were riveted together, as seen in Fig. 1, for the compression tests.

All compression tests were made in a 200,000-lb. Baldwin-Southwark hydraulic testing machine with a 1,000:1 Huggenberger extensometer mounted on each crown of the test specimen. The elongation was taken as the average reading of these two extensometers. The compression specimens, with their ends ground flat and parallel, were mounted on a self-aligning base in order to avoid eccentric loading.

Received May 18, 1942.

* Test Engineer.

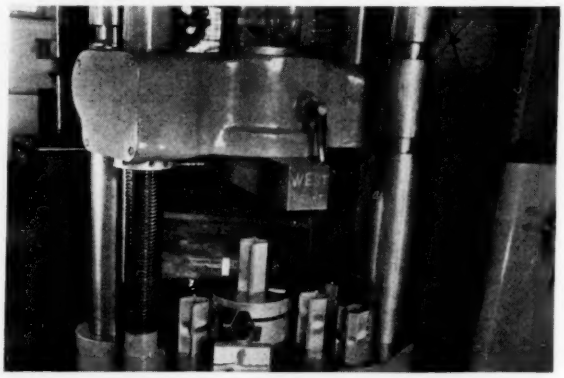

Fig. 1. Tests of prestretched extruded hat stiffeners compression setup.

All tension tests were made in a 5,000-lb. Tinius-Olsen hydraulic testing machine. Elongation was measured with a Riehle extensometer, which can be read to $^1/_{10,000}$ in. The tension specimens were of standard shape with the minimum section $^5/_8$ in. wide.

All heat-treating was done in a standard heat-treatment bath, with a difference in soaking time as the only variation of the heat-treatment. This bath is a solution of sodium nitrate and potassium nitrate held to a constant temperature of 930°F. Quenching was done in water at room temperature. After heat-treatment, in every case, the specimens were aged 24 hours or more before being stretched and three days or more before being static tested.

Stretching was the only method used for applying cold-work in this particular group of tests.

The conventional 0.2 per cent of permanent set was used as the criterion in determining the yield strength.

Discussion

The mechanical properties of extruded hats differ widely, both in the "as-received" condition and after a normal 45-min. heat-treatment. This difference was thought to be due to a variation of chemical properties until a check of two of the hats revealed almost identical quantities of the various constituents. Further heat-treatment of these two hats finally equalized them after nine hours of soaking time. The weaker of the two hats had an ultimate tensile strength of 65,000 lbs. per sq.in. after the first 45-min. heat-treatment. It still tested the same after nine hours. The other hat had an ultimate tensile strength of 77,000

TABLE 1
Mechanical Properties of 24ST Extruded Hat Stretched Successive Amounts

Stretch, Per Cent	U_T	Y_T	Y_C	X
0	71,000	46,700	45,700	−1,300
0.34	69,000	51,000	45,300	5,000
0.64	71,500	53,500	45,700	5,000
1.00	72,500	55,000	46,600	5,500
1.50	73,500	56,000	47,000	5,500
2.20	72,800	57,700	48,300	7,900
3.30	75,250	61,500	49,300	9,250
5.55	77,500	68,000	54,500	13,500
9.95	80,600	73,200	57,800	15,600

lbs. per sq.in. after the first 45 min. and 65,000 lbs. per sq.in. at the end of nine hours. Since the strength of the hats can be equalized by a prolonged heat-treatment, a uniform base line can be established for determining the amount of cold-work in any specimen. The establishment of a base line is a start, but the type of cold-work must also be known before the mechanical properties can be properly analyzed.

Cold-work increases the tensile yield strength of the material quite rapidly, but the ultimate unit strength is increased only in direct proportion to the change in cross-sectional area of the section. The tensile yield strength will approach the ultimate as the amount of work is increased until they are almost equal, then cold-working is stopped just short of the breaking point. Thus, the difference between the ultimate and the yield is an indication of the amount of work in the material. This difference averaged about 23,000 in all test specimens after heat-treatment. However, some of the cold-work may remain after heat-treatment, as evidenced by the nine-hour soaking time required in the case of the one specimen previously mentioned. The cold-work that remains in the material after a normal heat-treatment will be referred to here as "residual" cold-work in order to distinguish it from the cold-work that reduces the difference between the ultimate and the yield. In other words, residual cold-work is the amount of strength an extrusion has after a normal heat-treatment above what it would have had if given a prolonged heat-treatment.

SYMBOLS

U_T = tensile ultimate lbs. per sq.in.
Y_T = tensile yield lbs. per sq.in.
Y_C = compressive yield lbs. per sq.in.
X = $23{,}000 - (U_T - Y_T)$
Y_0 = Y_C when $X = 0$
Y_{T0} = Y_T when $X = 0$

DEVELOPMENT OF FORMULA

The compressive yield strength of these extrusions after a prolonged heat-treatment was found to be

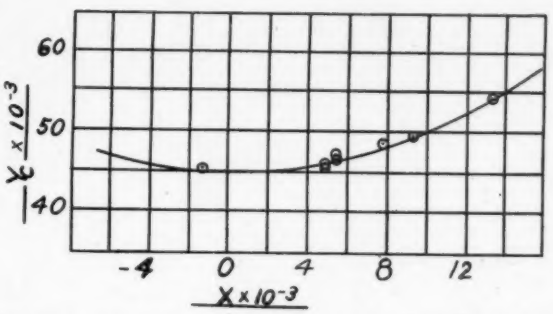

FIG. 2. Compressive yield curve of 24S-T extruded hat stretched successive amounts.

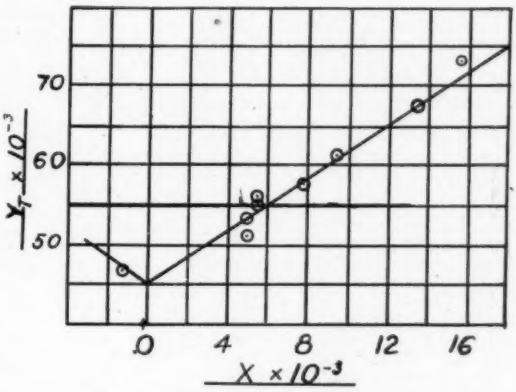

FIG. 3. Tensile yield curve of 24S-T extruded hat stretched successive amounts.

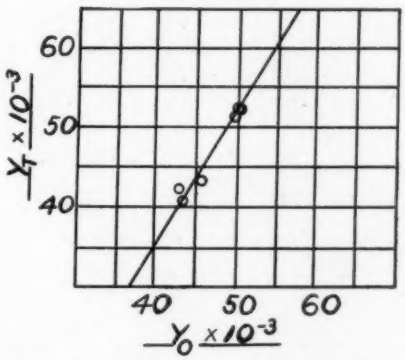

FIG. 4. Residual cold-work curve of 24S-T extrusions.

42,000 lbs. per sq.in. The total compressive yield strength at any time, regardless of its previous treatment, will therefore be 42,000 plus residual cold-work plus compressive gain due to other types of cold-work.

Since stretching was the only method used to cold-work these test specimens, it is the only type of cold-work combined with residual cold-work in these specimens.

Table 1 is a list of the mechanical properties of a single extruded hat that was first heat-treated and then stretched successive amounts. The compressive yield

TABLE 2
Mechanical Properties of 24ST Extruded Hats

U_T	Y_T	$U_T - Y_T$	X	$\frac{X^2}{19{,}000}$	Y_C (Calc.)	Y_C (Act.)	Error Per Cent	$\frac{X}{U_T} > 0.17$	$\frac{X}{U_T} < 0.17$
65,400	41,800	23,600	−600	19	43,500	43,700	+ 0.5	...	−0.01
63,600	42,500	21,100	1,900	190	42,750	44,000	+ 2.8	...	0.03
65,400	42,700	22,700	300	5	44,300	43,200	− 2.6	...	0
63,100	42,800	20,300	2,700	384	42,300	43,800	+ 3.4	...	0.04
61,500	44,300	17,200	5,800	1,770	41,450	44,000	+ 5.8	...	0.09
62,100	44,800	17,300	5,700	1,710	41,800	43,300	+ 3.5	...	0.09
61,400	44,400	17,000	6,000	1,895	41,400	42,100	+ 1.7	...	0.10
68,000	47,300	20,700	2,300	279	45,300	46,500	+ 2.6	...	0.03
63,500	48,700	14,800	8,200	3,540	43,400	43,200	− 0.5	...	0.13
64,600	49,200	15,400	7,600	3,040	43,800	42,900	− 2.1	...	0.12
63,300	49,000	14,300	8,700	3,980	43,500	42,500	− 2.4	...	0.14
77,000	50,000	27,000	−4,000	842	45,750	46,700	+ 2.0	...	−0.05
66,500	49,500	17,000	6,000	1,895	44,500	46,500	+ 4.3	...	0.09
77,100	49,600	27,500	−4,500	1,065	45,250	47,500	+ 4.7	...	−0.06
70,200	50,000	20,200	2,800	412	46,550	48,200	+ 3.4	...	0.04
73,300	51,000	22,300	700	26	48,900	50,800	+ 3.9	...	0.01
71,600	51,000	20,600	2,400	303	47,450	47,200	− 0.5	...	0.03
72,150	52,800	19,350	3,650	700	47,650	47,200	− 1.0	...	0.05
69,600	52,900	16,700	6,300	2,090	46,400	45,300	− 2.4	...	0.09
71,400	52,800	18,600	4,400	1,020	47,200	47,200	0	...	0.06
74,900	52,500	22,400	600	19	49,900	50,000	+ 0.2	...	0.01
74,700	52,800	21,900	1,100	64	49,600	51,200	+ 3.1	...	0.01
74,400	53,300	21,100	1,900	190	49,250	49,000	− 0.5	...	0.03
75,600	52,800	22,800	200	2	50,500	50,300	− 0.4	...	0
74,750	54,000	20,750	2,250	266	49,350	49,000	− 0.7	...	0.03
74,000	54,000	20,000	3,000	474	48,800	48,000	− 1.7	...	0.04
75,100	54,800	20,300	2,700	384	49,500	50,300	+ 1.6	...	0.04
76,100	54,200	21,900	1,100	64	50,450	50,500	+ 0.1	...	0.01
65,400	54,600	10,800	12,200	7,830	47,150	43,500	− 8.4	0.19	...
62,750	55,500	7,250	15,750	13,050	49,300	43,600	−13.1	0.25	...
62,500	56,400	6,100	16,900	15,070	50,650	44,800	−13.1	0.27	...
68,000	56,300	11,700	11,300	6,725	48,000	47,400	− 1.3	...	0.17
66,500	56,800	9,700	13,300	9,320	48,850	47,400	− 3.1	0.20	...
67,200	57,700	9,500	13,500	9,600	49,450	48,300	− 2.4	0.20	...
67,200	57,900	9,300	13,700	9,880	49,650	49,000	− 1.3	0.20	...
70,000	59,200	10,800	12,200	7,840	49,900	52,300	+ 4.6	0.18	...
66,500	59,700	6,800	16,200	13,800	52,100	55,500	+ 6.1	0.24	...
70,100	60,500	9,600	13,400	9,450	51,100	52,000	+ 1.7	0.19	...
74,900	60,700	14,200	8,800	4,075	50,500	50,300	− 0.4	...	0.12
74,100	61,500	12,600	10,400	5,690	51,000	49,600	− 2.8	...	0.14
70,500	61,900	8,600	14,400	10,900	52,300	50,000	− 4.6	0.20	...
69,000	62,300	6,700	16,300	14,000	56,050	49,000	−14.4	0.24	...
76,900	62,700	14,200	8,800	4,075	51,700	54,100	+ 4.4	...	0.11
71,700	65,300	6,400	16,600	14,500	55,750	52,300	− 6.6	0.23	...
71,600	65,600	6,000	17,000	15,200	56,200	50,400	−10.4	0.24	...
76,500	65,500	11,000	12,000	7,580	53,600	53,000	− 1.1	...	0.11
77,000	66,000	11,000	12,000	7,580	53,900	56,000	+ 3.7	...	0.11
74,000	66,700	7,300	15,700	12,980	56,000	50,000	−12.0	0.21	...

strength is plotted against "X" in Fig. 2. The resultant curve is a parabola that may be written as:

$$Y_C = (X^2/19{,}000) + Y_0 \qquad (1)$$

Y_0 is the residual cold-work plus the basic strength, and $X^2/19{,}000$ is the stretch type of cold-work.

The Y_T values of Table 1 plotted against "X" produce the curve in Fig 3 where for positive values of "X"

$$Y_T = Y_{T_0} + 1.7X \qquad (2)$$

and for negative values of "X"

$$Y_T = Y_{T_0} - 1.7X \qquad (3)$$

It can be seen from Fig. 2 that the difference between Y_0 and Y_C is very small for values of "X" up to ±1,000. Since Y_0 is the compressive yield when "X" is zero and since Y_{T_0} is the tensile yield at the same point, the connecting link between Y_0 and Y_T

TABLE 3
Mechanical Properties of 24ST Alclad Hats

U_T	Y_T	$U_T - Y_T$	X	$\frac{X^2}{19{,}000}$	Y_C (Calc.)	Y_C (Act.)	Error Per Cent	$\frac{X}{U_T} > 0.17$	$\frac{X}{U_T} < 0.17$
65,600	47,300	18,300	4,700	1,160	43,750	44,200	+1.0	...	0.07
67,750	51,000	16,750	6,250	2,060	45,300	44,000	−3.0	...	0.09
68,100	52,000	16,100	6,900	2,510	45,700	45,000	−1.6	...	0.10
66,600	52,500	14,100	8,900	4,070	43,500	44,600	+2.5	...	0.13
66,900	56,200	10,700	12,300	7,960	48,150	46,500	−3.5	0.18	...
67,900	53,300	14,600	8,400	3,710	46,150	46,300	+0.3	...	0.12
66,400	53,300	13,100	9,900	5,160	46,050	45,300	−1.7	...	0.15
68,000	53,800	14,200	8,800	4,075	46,350	46,200	−0.3	...	0.13
68,100	54,400	13,700	9,300	4,550	46,700	45,500	−2.6	...	0.14
67,800	54,400	13,400	9,600	4,850	46,700	47,400	+1.5	...	0.14
68,300	56,000	12,300	10,700	6,025	47,700	47,800	+0.2	...	0.16
68,750	56,000	12,750	10,250	5,530	47,650	49,600	+3.9	...	0.15
68,600	56,300	12,300	10,700	6,025	47,900	48,500	+1.2	...	0.16
69.000	56,400	12,600	10,400	5,700	47,950	46,700	−2.7	...	0.15

can be obtained by plotting Y_0 against Y_{T_0}. Choosing values of "X" less than 1,100 from Table 2 and plotting the corresponding Y_{T_0} (calculated from Eqs. (2) and (3)) values against Y_0, the curve in Fig. 4 is obtained. The equation for this curve is:

$$Y_0 = 0.6Y_{T_0} + 19{,}000 \qquad (4)$$

Combining Eqs. (1), (2), and (4), and Eqs. (1), (3), and (4)

$$Y_C = (X^2/19{,}000) \mp 1.02X + 0.6Y_T + 19{,}000 \qquad (5)$$

The sign of the term "$1.02X$" in the above equation is negative when "X" is positive and positive when "X" is negative. The product of this term is, therefore, always negative and Eq. (5) can be written as:

$$Y_C = (X^2/19{,}000) - 1.02X + 0.6Y_T + 19{,}000 \qquad (6)$$

if the numerical value only of "X" is used.

PROOF OF FORMULA

Tables 2 and 3 list the actual tensile and compressive strengths, together with the calculated compressive strength, of all of those hats on which both tension and compression tests were run. Table 2 has a few cases where the error in calculating the compressive yield is quite high. However, only those with both a low ultimate and high value for X have this large error. On this basis a limiting factor can be set up by using the ratio of X/U_T. This ratio was set at $X/U_T \leq 0.17$ as a safe limit. This allows a maximum error of 5.8 per cent in this series of tests. As a further check on the probable cause of error, a 20-ft. length of extruded hat was tested for variation in tensile strength. It was first heat-treated and stretched $1\frac{1}{2}$ per cent. Then ten tensile samples were cut from sections throughout its length. The tensile ultimate of these ten specimens varied ±4 per cent and the tensile yield ±3 per cent from the average.

LIMITATIONS OF FORMULA

Because it is an expression of residual cold-work and the stretch type of cold-work, this formula will not apply to precompressed specimens. However, it can be used for determining the original compressive strength of a specimen that has failed in compression. The high compressive stress, applied just before failure, on such a specimen will increase the compressive yield strength but will not appreciably affect the tensile properties.

Since the thickest hat section tested in the development of this formula was 0.128 in., and the thinnest 0.072 in., it should not be used outside of these limits, and because of the variation of tensile properties in a single stringer, it cannot be expected to give results closer than ±4 per cent. It should not be relied upon if X_{U_T} is greater than 0.17.

APPLICATION OF FORMULA

In order to take advantage of the full strength of extruded hats in aircraft construction, the following procedure is suggested: All extrusions intended for use in stringer combinations would be numbered and weighed separately and tensile samples cut from each. The tensile samples would be tested and the compressive strength of each extrusion calculated by means of Eq. 6. (The calculated value should be reduced 4 per cent to allow for material variations in the stringer.) The average area of each extrusion can be calculated from its weight and length. Then the actual compressive strength in pounds would be figured and the extrusions sorted according to their respective strengths.

The designer, knowing the actual strength of the stringers, would place the strongest stringers in the region of highest stress. For example, the shear lag across a wing puts a higher load on the stringers nearest the spars. These stringers would therefore be taken

from the high-strength group and the weaker ones would be placed farther from the spars.

Conclusions

24ST aluminum alloy extrusions have a potential compressive yield strength of 56,000 lbs. per sq.in. but, because of variation in mechanical properties, have a design allowable strength of only 38,000 lbs. per sq.in. This design allowable can be increased up to 30 per cent if a tensile test is made of each extrusion and the true compressive strength of the extrusion determined by Eq. 6. Then, by weeding out the weakest sections or placing them at points of lowest stress, the maximum compressive yield strength of the plate stringer combination can be realized.

Bibliography

[1] Jackman, K. R., *Modern Aircraft Materials and Their Testing*, S.A.E. Journal, November, 1940.

[2] Holt, M., and Hartmann, E. C., *Increasing the Strength of Aluminum Alloy Columns by Prestressing*, N.A.C.A. T.N. No. 618, 1937.

[3] Templin, R. L., and Sturm, R. G., *Some Stress Strain Studies of Metals*, Journal of the Aeronautical Sciences, Vol. 7, No. 5, March, 1940.

[4] Templin, R. L., Sturm, R. G., Hartmann, E. C., and Holt, M., *Column Strength of Various Aluminum Alloys*, Technical Paper No. 1, Aluminum Research Laboratories, 1938.

[5] Jackman, K. R., *Strengthening Aluminum for Aircraft Structures*, Metal Progress, Vol. 40, No. 1, July, 1941.

[6] Fischel, J. Robert, *The Compressive Strength of Thin Aluminum Alloy Sheet in the Plastic Region*, Journal of the Aeronautical Sciences, Vol. 8, No. 7, August, 1941.

Letter to the Editor

Dear Sir:

An inspection of Eqs. (1) to (4) of my paper entitled "Proportioning a Canard for Longitudinal Stability and Safety Against Stall," published in the December, 1942, issue of the Journal of the Aeronautical Sciences, leads to a further conclusion of particular interest which was not listed at the end of that paper.

In order to do away with the limitation of tail length, and therefore, of range of allowable c.g. locations, which is one of the major disadvantages of the canard, the tail surface should be designed in such a way that its lift coefficient would be independent of the angle of attack of the airplane. In this case the derivative of the term containing the tail length and tail surface characteristics would be zero, and these items would be eliminated from Eqs. (3) and (4). Then the static longitudinal stability of the airplane would be independent of the tail length and the most rearward allowable position of the c.g. for stability would be as far back as it would be in the tailless airplane.

This could be attained by attaching the horizontal tail surfaces to the body of the airplane by means of an articulation that would leave the tail surface free to rotate about a transversal axis. Then the horizontal tail surface, if so designed as to be longitudinally autostable, would always remain at its angle of attack of equilibrium, regardless of the angle of attack of the rest of the airplane. The pilot, through the control stick and tabs or other auxiliary surfaces attached to the tail, would control the angle of attack of equilibrium of the latter, not its incidence with respect to the rest of the airplane.

This type of canard would still be automatically safe against stall if h_r (Eq. (5)) was assumed as the most rearward c.g. location. However, since such a horizontal tail surface would be fully controllable at all angles of attack of the airplane, h_0 could be assumed as the most rearward allowable c.g. location; this would provide a further increase of the range of allowable c.g. displacements.

Joseph V. Foa
Chief Engineer
American Aero-Marine Industries, Inc.

Graphical Analysis of Delay of Response in Air-Speed Indicators

KALMAN J. DEJUHASZ*†
The Pennsylvania State College

SUMMARY

The delay of response of the pneumatic system of the air-speed indicator is analyzed by a graphic method and illustrated by an example of an actual installation, with various simplifying assumptions and for various modifications of the system. The results are compared with those previously obtained by mathematical analysis. The results of mathematical analysis agree well with those obtained by graphic analysis for those pneumatic systems in which the inertia of the moving air column is small in comparison with the resistance to flow; in other cases important deviations have been found. The design data for minimum delay have been determined. Applicability of the method for any given law of impressed pressure change is illustrated by examples.

THE LIFT OF AN AIRPLANE is dependent on the air speed; therefore it is of prime importance that the pilot should be informed at all times of the accurate value of the speed. For this purpose there is used an air-speed indicator,[1] which is based on the principle that the difference of pressure Δp between the dynamic pressure at a pitot head and the static pressure of the surrounding atmosphere is proportional to the square of the air speed v_a according to the equation

$$\Delta p = \rho v_a^2/2$$

where ρ is the density of the air.

The pressure difference is measured by a sensitive pressure gauge, usually of the aneroid capsule type, which is mounted on the instrument board in the fuselage. The pitot element is placed in the undisturbed air stream at a distance of several feet from the pressure gauge. The two are connected with a tubing which, in actual installations, is about 30 to 50 ft. long. A damping orifice is sometimes incorporated in the system in order to damp out vibrations. These elements constitute a pneumatic system, illustrated in Fig. 1, comprising volumes and resistances to flow. Because of the presence of these elements, any change of pressure occurring at the pitot head will not be communicated to the pressure gauge instantaneously but with a certain delay. Another source of delay is the inertia of the moving parts of the pressure gauge itself, but this is small in comparison with the delay caused by the pneumatic system and will not be considered in the present treatment.

The purpose of this paper is to (1) determine the delay in terms of the design data of the pneumatic system and (2) find the dimensions of the pneumatic system whereby the minimum delay is attained.

STATEMENT OF THE PROBLEM

In the present treatment the altitude and temperature, and hence the static pressure and density, are assumed to be constant. In order to simplify the problem it is assumed that the air speed changes suddenly, as in a gust, involving an instantaneous change of dynamic pressure at the pitot head from an initial value p_1 to a new value p_2 (Fig. 2). Then the pressure p in the pressure gauge will not assume the new dynamic pressure instantaneously but will approach it gradually as some function of time $p = f(t)$; hence during a certain time it will not indicate the air speed correctly. It is our purpose to determine the function $p = f(t)$.

FIG. 1

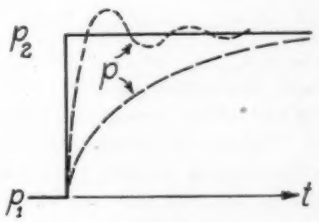

FIG. 2

FIG. 1. Pneumatic system of air-speed indicator. *P*, pitot head; *D*, damping orifice; *L*, tubing; *A*, aneroid capsule. FIG. 2. Response of air-speed indicator to sudden pressure change. Dynamic pressure increases suddenly from value p_1 to value p_2. The air-speed indicator indicates a pressure $p = f(t)$, which may be a periodic or aperiodic function of time.

This problem has been treated in the engineering literature experimentally and by mathematical analysis, both for related aircraft instruments[3,6-9] and specifically for air-speed meters.[2,4,5] In the usual mathematical analysis, however, rather drastic simplifying assumptions are involved. In the present paper a graphic method will generally be used which permits a closer approximation to the actual conditions and possesses the advantage of simplicity and clarity of presentation of the phenomena involved. Similar graphic methods have been applied to other problems of tran-

Presented at the Radio and Instruments Session, Eleventh Annual Meeting, I.Ae.S., New York, January 25–29, 1943.

* Professor of Engineering Research, School of Engineering.

† The author expresses his appreciation to Drs. W. G. Brombacher and C. S. Draper for their comments and suggestions and to Mr. A. Yorgiadis for the careful drawings and for checking the calculations.

sient phenomena in elastic systems, but these have not been applied to problems of aircraft instruments so far as it could be ascertained.

Basic Relationships and Assumptions

(a) The change of state of air is assumed to be adiabatic, for which $(\rho/\rho_0)^\kappa = p/p_0$; $d\rho/\rho_0 = dp/\kappa p_0$; $\kappa = 1.4$; $p_0 = 10{,}000$ kg./m.^{2} In the present case the pressure change is assumed to be small in comparison with the absolute value of pressure; therefore the reference pressure p_0 is assumed to be constant. The value $\kappa p_0 = 14{,}000$ kg./m.^{2} is the "modulus of volume elasticity" of the air.

(b) A container is characterized by its "capacity" C, which is the volume rate at which the medium enters into it or leaves it per unit of pressure change in the container and which can be expressed by the equation:

$$C = \frac{d(V\rho)}{\rho dp} = \frac{\rho dV}{\rho dp} + \frac{V d\rho}{\rho dp}$$

For a rigid container $dV/dp = 0$; therefore the capacity is:

$$C_{\text{rigid}} = V/\kappa p_0$$

For an elastic container, the volume of which is a linear function of the pressure:

$$V_{\text{elastic}} = V_0 + (dV/dp)p = V_0 + Ap$$

the capacity can be expressed as

$$C_{\text{elastic}} = (V_0/\kappa p_0) + A = \frac{1}{\kappa p_0}(V_0 + A\kappa p_0) = \frac{1}{\kappa p_0}(V_{\text{equivalent}})$$

The term $V_{\text{equivalent}} = V_0 + A\kappa p_0$ is the volume of a rigid container having the same capacity as the elastic container and will be termed "equivalent rigid volume."

(c) The pressure drop due to an orifice or pipe is a function of the flow velocity $\Delta p = f(v)$, which is a simple proportionality in the case of laminar flow. In the present case the flow velocity is low and the diameters are small; in other words, the Reynolds number is low; therefore laminar flow is assumed to exist for which the pressure drop is expressed by the Hagen-Poiseuille formula: $\Delta p = (32\,\eta L/d^2)v$; L = length; d = diameter; v = flow velocity; η = absolute viscosity of air. The volume flow per second, q, can be expressed:

$$q = vF = (d^2F/32\,\eta L))\,\Delta p = \Delta p/R;$$
$$R = 32\,\eta L/d^2F = \text{resistance of pipe}$$

Symbols with index L will refer to the tubing; with index a, to the aneroid capsule; and with index D, to the damping capillary orifice.

Mathematical Analysis

It is assumed that all the volumes, capacities, and resistances in the system are combined into one total volume, total capacity, and total resistance, for which: $V = V_L + V_a$; $C = V/\kappa p_0$; $R = R_L + R_D$. Then for a q volume flow per second it can be written:

$$\Delta p = qR;\quad q\,dt = C\,dp$$

Broadly, then, the mathematical analysis treats the problem in the simple form: A compact container C with a negligible length dimension, Fig. 3a, communicates with the outside atmosphere through an orifice having the resistance R; the pressure of the outside atmosphere changes instantaneously from p_1 to p_2; the pressure p in the container is to be determined as a function of time $p = f(t)$. Thus, the inertia of the flowing air column is neglected, and it is assumed that at any given instant the pressure at all points in the pneumatic system is the same. It can be written: $Cdp = [(p_2 - p)/R]dt$; hence, $dp/(p_2 - p) = dt/CR$. After integration the exponential relationship is obtained:

$$p_2 - p = (p_2 - p_1)e^{-t/RC}$$

which is depicted in Fig. 3b.

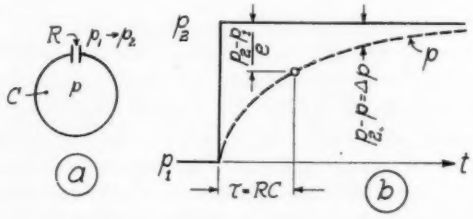

FIG. 3. (a) Substitute pneumatic system as treated by mathematical analysis; C, capacity; R, resistance. (b) Change of pressure in substitute pneumatic system.

The product $RC = \tau$ has the dimension of time and is termed the "time constant" or "characteristic time" of the system. It characterizes the rapidity of response of the system to a change of pressure, and its significance is: that after the elapse of time τ the error, Δp, will be $1/e = 0.368$ times its initial value. (After the elapse of time 2τ, the error is 13 per cent; after time 3τ, it is 5 per cent; after time 4τ, it is 1.8 per cent; and after time 5τ, it is 0.67 per cent.)

It will be noted that this formula is analogous to that describing the electrical phenomenon of charging and discharging a condenser through an ohmic resistance: For a sudden change of the terminal voltage from E_1 to E_2 it can be written:

$$E_2 - E = (E_2 - E_1)e^{-t/RC}$$

whereby $p_2 - p$ is analogous with the voltage difference, C with the capitance, and R with the resistance in the circuit, Fig. 4.

It is evident that the mathematical analysis represents a rather rough approximation to the actual conditions, because it assumes in the system an infinitely great velocity of propagation of the pressure change

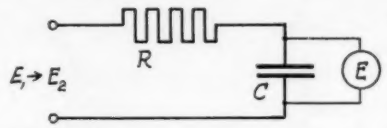

FIG. 4. Electrical analogy of pneumatic system; E_1, E_2, impressed voltage; R, ohmic resistance; C, condenser; E, voltage across condenser.

and neglects the effect of the momentum of the air column. Mathematical difficulties prevent taking these effects into consideration by mathematical analysis, but it can be done with comparative ease by graphic analysis.

GRAPHIC ANALYSIS

The equalization of pressure in air-speed indicators belongs in the group of transient phenomena in elastic columns. These have been treated by graphic analysis in previous publications[10] where also the full derivation is given. For this reason at this place only the main conclusions, as applied to the present problem, will be summarized.

The graphic analysis deals with "disturbances," which term denotes a change of velocity or of pressure, impressed on a fluid column at some point in the system as a function of time. In the present case the instantaneous change of pressure at the pitot head, from p_1 to p_2 is a disturbance that is representable in a t-p diagram as a step function.

In graphic analysis the elements of the system and the phenomena are represented as functions of two of the following variables: pressure p, velocity v, time t, and location x. The following relations hold good:

(1) In a system a disturbance, originated at one point x_0 at a certain instant of time t_0, is propagated along the system with a constant velocity a termed the "velocity of propagation" or "acoustic velocity." Therefore for the location x of the disturbance at an instant t of time it can be written:

$$\frac{x - x_0}{t - t_0} = \frac{\Delta x}{\Delta t} = \pm a = \tan(\pm\varphi)$$

This relationship can be represented in a t-x chart by a straight line forming an angle φ with the t-axis. The sign is positive or negative depending on whether the disturbance travels forward (increasing x with increasing time) or backward (decreasing x with increasing time). For air the mean value of the velocity of propagation is: $a = 338$ m./sec.

(2) For a finite length of pipe the value $L/a = T$ is an important property denoting the time interval necessary for a disturbance to travel from one end of the pipe to the other.

(3) In a frictionless pipe a change of pressure is always accompanied by a proportionate change of velocity and vice versa, i.e.,

$$\Delta p / \Delta v = \text{const.} = \pm \kappa p_0 / a$$

It is convenient to use, instead of the linear velocity v, the volume velocity of flow $q = Fv$, with which it can be written:

$$\frac{\Delta p}{\Delta q} = \frac{\Delta p}{F \Delta v} = \text{const.} = \pm \frac{\kappa p_0}{Fa} = \tan(\pm\alpha)$$

This relationship can be represented in a q-p chart by straight lines forming an angle α with the q-axis. The expression $\kappa p_0/Fa$ may be termed the "wave constant," and its value for air is:

$$\kappa p_0/Fa = 14{,}000/338F = (41.5/F) \text{ kg. sec./m.}^5$$

(4) The resistance of an orifice or a pipe can be expressed by the pressure drop $p_2 - p$ necessary to produce a certain rate of flow q, i.e.,

$$(p_2 - p)/q = R = \tan\rho$$

which can be represented in the q-p chart by a straight line forming an angle ρ with the q-axis and passing through the $q = 0$, $p = p_2$ point. For turbulent flow the function is quadratic and can be represented by a parabola. The function needs not be stated in mathematical form but can be represented by a curve expressing the flow-velocity, pressure relationship, which may be an experimentally determined one.

APPLICATION OF GRAPHIC ANALYSIS TO THE AIR-SPEED INDICATOR

In possession of the above relationships an air-speed meter will be analyzed under various assumptions and modifications. The data of the air and of the air-speed indicator[5] (installation in the German Ju 52 airplane) are:

Air

Modulus of elasticity = $\kappa p_0 = (1.4 \times 10^4/\text{m.}^2)$ kg.
Acoustic velocity = $a = 338$ m./sec.
Wave factor = $\kappa p_0/a = (41.5/\text{m.}^3)$ kg. sec.
Kinematic viscosity = $\eta = (1.83 \times 10^{-6}/\text{m.}^2)$ kg. sec.
Density = $\rho = (0.123/\text{m.}^4)$ kg. sec.^{2}

Aneroid capsule

Volume [at $p_0 = (10^4/\text{m.}^2$ kg.] = $V_0 = 11 \times 10^{-6}$ m.^{3}
Volume increase [at $\Delta p = (200/\text{m.}^2)$ kg.] = $\Delta V = 0.7 \times 10^{-6}$ m.^{3}

$$\Delta V / \Delta p = A = 35 \times 10^{-10} \text{ m.}^5/\text{kg.}$$

Equivalent rigid volume = $V_{\text{equivalent}} = (11 \times 10^{-6} + 1.4 \times 10^4 \times A) = 60 \times 10^{-6}$ m.^{3}
Equivalent capacity = $C_a = V_{\text{equivalent}} / \kappa p_0 = 43 \times 10^{-10}$ m.^{5}/mg.
Wave factor = $\kappa p_0/aF = (\kappa p_0 / V_{\text{equivalent}})(L/a) = 0.69 \times L$

Tube

Length = $L_L = 10$ m.

Diameter = $d_L = 6 \times 10^{-3}$ m.
Cross-sectional area = $F_L = d_L^2 \pi/4 = 28.3 = 10^{-6}$ m.^{2}
Volume = $V_L = L_L F_L = 283 \times 10^{-6}$ m.^{3}
Capacity = $C_L = V_L/\kappa p_0 = 202 \times 10^{-10}$ m.^{5}/kg.
Resistance = $R_L = 32\eta L_L/d_L^2 F_L = (0.575 \times 10^6/$ m.^{5}) kg. sec.
Interval of traverse = $L_L/a = 0.0296$ sec.

Damping capillary

Length = $L_D = 0.2$ m.
Diameter = $d_D = 0.90 \times 10^{-3}$ m.
Resistance = $R_D = (22.7 \times 10^6/\text{m.}^5)$ kg. sec.

For this system the calculated time constant is:

$$\tau = (R_D + R_L)(C_L + C_a) = 23.27 \times 245 \times 10^{-4} = 0.57 \text{ sec.}$$

and the pressure function is:

$$p_2 - p = (p_2 - p_1)e^{-t/\tau}$$

(a) In the graphic analysis, as a first approximation, it will be assumed that the volume of the capsule is added to the tube in the form of an additional length, so that the total volume of the assumed tube is equal to that of the actual tube plus the volume of the capsule. Furthermore, the resistance of the pipe is added to that of the damping orifice. In other words, the approximation will be similar to that used in the mathematical analysis, with the refinement, however, that the finite length of the system and the inertia of the air column are taken into consideration.

The length of the substitute tube will be $L' = (283 + 60)/28.3 = 12.1$ m. and its time interval $L'/a = 0.0358$ sec. The inertia of the air column is represented by the angle α for which

$$\tan(\pm\alpha) = \Delta p/\Delta q = \kappa p_0/Fa = (\kappa p_0/V)(L/a) = T/C = (1.47 \times 10^6/\text{m.}^5) \text{ kg. sec.}$$

The resistance of the system comprises that of both the damping orifice and the pipe L and is characterized by the angle ρ for which:

$$\tan\rho = (p_2 - p)/q = R = (23.27 \times 10^6/\text{m.}^5) \text{ kg. sec.}$$

These values of α and ρ are represented in the q-p chart, and the construction is carried out as shown in Fig. 5. A pressure difference $\Delta p = 100$ kg./m.^{2} is assumed corresponding to an air-speed increase from 160 km. per hour to 216 km. per hour.

On this Fig. 5 are shown: (a) the t-x chart on which every point represents a certain location in the system as defined by the x-ordinate and an instant of time as represented by the abscissa. By lines having the slope $\tan(\pm\varphi)$, running from the orifice end to the closed end, this coordinate system is divided into triangular zones; the condition of the velocity and pressure in each zone is defined by a similarly numbered point in the q-p chart. (b) The q-p chart contains the $R = \tan\rho$ line representing the combined resistances and the $\pm\tan\alpha$ lines representing the flow conditions in the tube. After the elapse of successive L/a intervals the disturbance wave arrives alternately at the orifice end (characterized by the $R = \tan\rho$ line) and at the closed end (i.e., capsule end, characterized by $q = 0$). These successive conditions are defined by points, 1, 2, 3, ... in the q-p chart and are valid for the zones marked 1, 2, 3, ... in the t-x chart. (c) The history of pressure chart for the pitot end of the tube (characterized by the step function rising from p_1 to p_2 instantaneously) and the capsule end of the tube (characterized by a stepwise rising pressure line, having steps of decreasing magnitude as the time progresses).

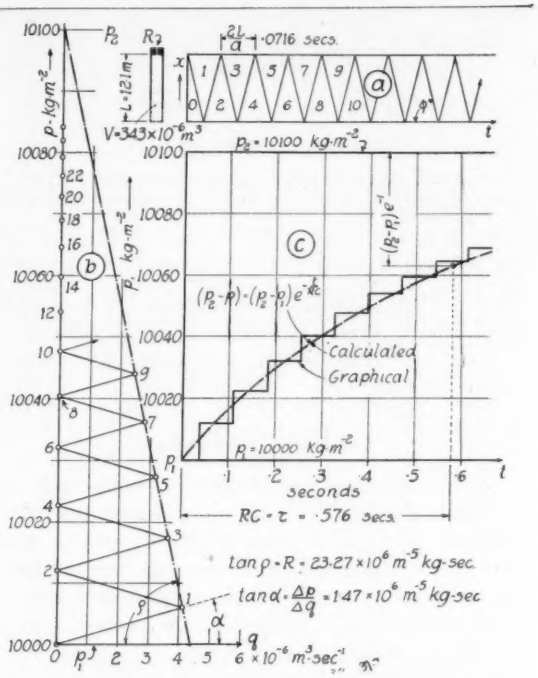

FIG. 5. Graphic analysis of Ju 52 air-speed indicator installation, assuming an added tubing length, so that total tubing volume equals the system volume. (a) t-x diagram; (b) q-p diagram; (c) history diagram of pressure at pitot head (step function suddenly rising from p_1 to p_2), and at capsule (pressure rising in steps of $2L/a$ duration, with steps of decreasing magnitude); calculated exponential pressure curve is also drawn in.

The calculated exponential pressure curve is also drawn in this diagram and shows a close argument with the graphically obtained stepped line.

The sum of the steps up to a certain time can also be calculated as follows: After the elapse of $2L/a = 2T$ time the pressure at the closed end of the tube will increase by $2\Delta p_1$, for which

$$\Delta p_1 = [(p_2 - p_1) - \Delta p_1]\frac{\tan\alpha}{\tan\rho}; \quad \frac{\tan\alpha}{\tan\rho} = \frac{T}{CR} = m$$

therefore the "error" will be

$$p_2 - p_{2T} = [(1 - m)/(1 + m)](p_2 - p_1)$$

Similarly, after the elapse of $4T$ time the error will be

$$p_2 - p_{4T} = [(1 - m)/(1 + m)]^2 (p_2 - p_1)$$

and after the elapse of $t = 2nT$ time the error will be

$$p_2 - p_{2nT} = [(1 - m)/(1 + m)]^n (p_2 - p_1)$$

It can be shown that as the length of the container is reduced (keeping the volume constant), i.e., the interval T is reduced, then in the limiting case the stepped function will assume the form of an exponential function. Namely, substituting $T = t/(2n)$ in the above equation:

$$p_2 - p_t = \left[\frac{1 - (t/2\ CR)\ (1/n)}{1 + (t/2\ CR)\ (1/n)}\right]^n (p_2 - p_1)$$

is obtained, and in the limiting case, lim $L = 0$; lim $T = 0$; lim $n = \infty$; therefore

$$\left[\frac{1 - (t/2\ CR)(1/n)}{1 + (t/2\ CR)(1/n)}\right]^n = e^{-t/CR}$$

hence

$$p_2 - p_t = (p_2 \quad p_1)e^{-t/RC}$$

which is the same expression as that obtained by the mathematical analysis.

(b) A closer approximation to the actual conditions can be realized by treating the capsule as a distinct element (i.e., not to absorb its volume in the tube volume, as it was done under (a)). In Fig. 6 it is assumed that the capsule is represented by a tube having the same length as the connecting tubing and having a cross-sectional area such that the volume is the same as the capsule volume. The wave factor of the capsule will be:

$$L_a = 10 \text{ m.}$$

$$\tan \beta = \frac{\Delta p}{\Delta q} = (\kappa p_0/V)\ \frac{L_a}{a} = (6.9 \times 10^6/\text{m}^5.)\ \text{kg. sec.}$$

The construction is shown for the t-x chart, the q-p chart, and for the history chart for the pressure, for both the pitot end and the capsule end. It is seen that the stepwise rising pressure line exhibits a somewhat different character from that obtained for assumption (a), but the calculated exponential pressure function still closely coincides with the graphic result.

(c) A still closer approximation to the actual conditions can be realized by treating the capsule as a tube shorter than the connecting tubing. In Fig. 7 it is assumed that the capsule length is one-third of the tube length, and correspondingly the cross section is greater than in the former case. The wave factor will be:

$$L_a = 3.33 \text{ m.}$$

$$\tan \beta = \frac{\Delta p}{\Delta q} = (2.3 \times 10^6/\text{m}^5.)\ \text{kg. sec.}$$

The construction is shown in Fig. 7a for the t-x chart, Fig. 7b, the q-p chart, and Fig. 7c for the history

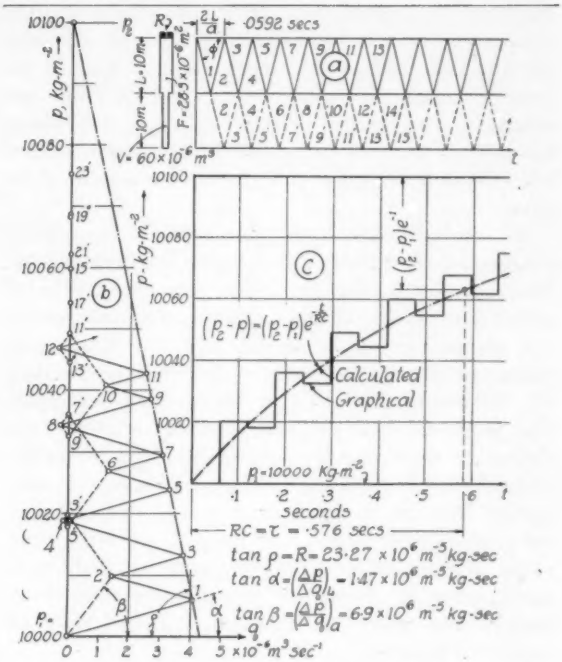
·0592 secs
Calculated
Graphical
seconds
RC = τ = ·576 secs
tan ρ = R = 23·27 × 10⁶ m⁻⁵ kg·sec
tan α = (ΔP/Δq)_L = 14·7 × 10⁶ m⁻⁵ kg·sec
tan β = (ΔP/Δq)_a = 6·9 × 10⁶ m⁻⁵ kg·sec

FIG. 6. Graphic analysis of Ju 52 air-speed indicator installation, assuming a capsule length equal to the tube length. (a) t-x diagram; (b) q-p diagram; (c) history diagram of pressure at pitot head (step function suddenly rising from p_1 to p_2), and at capsule (pressure rising and falling in steps of $2L/a$ duration); calculated exponential pressure curve is also drawn in.

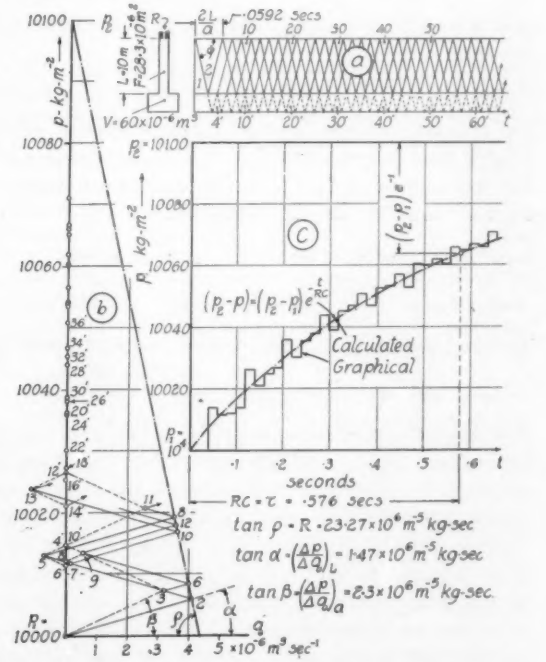
·0592 secs
Calculated
Graphical
seconds
RC = τ = ·576 secs
tan ρ = R = 23·27 × 10⁶ m⁻⁵ kg·sec
tan α = (ΔP/Δq)_L = 14·7 × 10⁶ m⁻⁵ kg·sec
tan β = (ΔP/Δq)_a = 23 × 10⁶ m⁻⁵ kg·sec.

FIG. 7. Graphic analysis of Ju 52 air-speed indicator installation, assuming a capsule length equal to one-third of the tube length. (a) t-x diagram; (b) q-p diagram; (c) history diagram of pressure at pitot head (step function suddenly rising from p_1 to p_2), and at capsule (pressure rising and falling in steps of $2L/3a$ duration); calculated exponential pressure curve is also drawn in.

chart for the pressure, for both the pitot end and the capsule end. It is seen that the stepwise changing pressure line exhibits a different character than in the formerly treated assumptions (a) and (b), but the calculated exponential pressure function still passes through the steps of the graphically obtained stepped line and can be regarded as the faired, mean value of the latter.

(d) Actually, the length dimension of the capsule is a much smaller fraction of the tube length than it has been assumed under (c). With the expenditure of added labor and attention to the graphic construction but without any inherent difficulty, the actual condition could be realized with any desired approximation by the procedure shown in the previous examples. This would be, however, only of academic interest because even the foregoing examples show that the mathematical analysis gives a satifactory approximation for a system with the design data as given. Nevertheless, the graphic construction is of interest, since it gives a closer approximation of the phenomenon and, so to speak, gives an insight into the microstructure of the phenomenon which the mathematical analysis is incapable of providing.

(e) In the example treated under (a), (b), and (c) the relative magnitude of the resistance and inertia was such that

$$\frac{\tan \alpha}{\tan \rho} = \frac{T}{RC} = [(L/a)/(RC)] < 1$$

It is of interest to investigate a case of such characteristics that

$$\tan \alpha/\tan \rho = (T/RC) > 1$$

For this purpose the formerly assumed system will be treated with the modification that the damping capillary is removed, so that the only resistance to flow will be that caused by the tube itself, i.e.,

$$\tan \rho = R = (0.575 \times 10^6/\text{m.}^5) \text{ kg. sec.}$$

$$\tan \alpha/\tan \rho = 1.47/0.575 = 2.56$$

In this case the calculated time constant will be:

$$\tau = RC = 0.575 \times 245 \times 10^{-4} = 0.014 \text{ sec.}$$

The graphic construction is shown in Fig. 8, giving the t-x and q-p charts, and also the history chart for the pressure, for both the pitot end and the capsule end. In the latter the calculated exponential pressure curve is also included. It is seen that in this case the actual phenomenon will not be an aperiodically damped function of time as represented by the exponential pressure curve but a periodically damped function as represented by the graphically obtained stepped line exhibiting steps above and below the true pressure p_2 line, the steps having decreasing magnitude as the time progresses.

(f) Particular interest attaches to the case in which:

$$\tan \alpha = \tan \rho; \quad L/a = T = RC$$

and which is shown in graphic representation in Fig. 9. It is readily seen that in this case complete equalization of pressure will occur at the end of the first L/a interval. Such a system possesses the least conceivable delay of response, which is the time necessary for the "new" air pressure to be propagated to the closed end (i.e., capsule end) of the tube. The phenomenon in this case is analogous to a critically damped vibration.

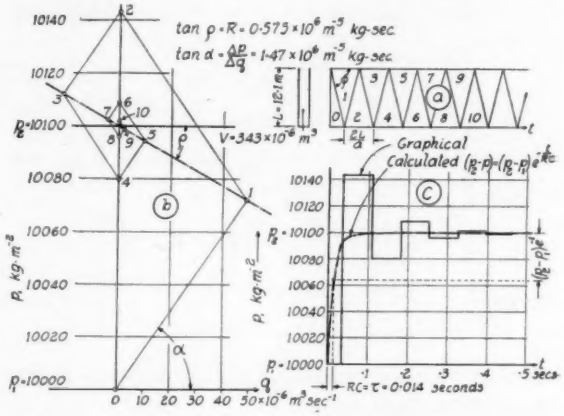

FIG. 8. Graphic analysis of Ju 52 air-speed indicator installation, assuming that the damping orifice is removed and assuming an added tube length, so that the total tubing volume equals the system volume. (a) t-x diagram; (b) q-p diagram; (c) history diagram of pressure at pitot head (step function suddenly rising from p_1 to p_2), and at capsule (pressure fluctuating above and below the true pressure line p_2 with decreasing magnitude as time progresses); calculated exponential pressure curve is also drawn in.

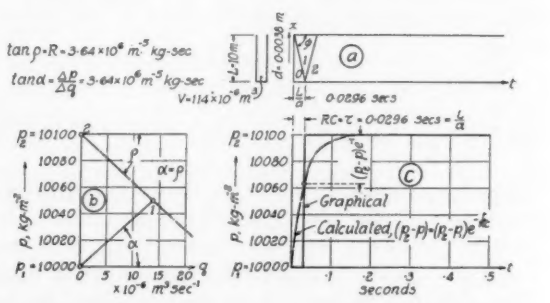
tan ρ = R = 3·64 × 10⁶ m⁻⁵ kg-sec
tan α = ΔP/Δq = 3·64 × 10⁶ m⁻⁵ kg-sec
V = 114 × 10⁻⁶ m³
RC = τ = 0·0296 secs = L/a
Graphical
Calculated (p₂-p) = (p₂-p₁)e^(-t/RC)
seconds
p, kg-m⁻²
q
t
α = ρ

FIG. 9. Graphic analysis of Ju 52 air-speed indicator installation, assuming a wave factor equal to the resistance. (a) t-x diagram; (b) q-p diagram; (c) history diagram of pressure at pitot head (step function suddenly rising from p_1 to p_2), and at capsule (step function suddenly rising from p_1 to p_2); calculated exponential pressure curve is also drawn in.

(g) If the volume of the capsule is negligible in comparison with the tube volume and, if there is no damping resistance, then this optimum condition, i.e., least delay, will be obtained when the tube length and diameter are in the following relationship:

$$L = aRC = a(32\ \eta\ L/d^2F)(FL/\kappa p_0)$$

$$d^2 = 32\ \eta(a/\kappa p_0)L$$

$$d = 1.2 \times 10^{-3} \sqrt{L}$$

For example, for a length of 10 m. the optimum diameter is 3.8 mm.

It has to be borne in mind that the above results are based on assumptions that may not always be fulfilled practically. A streamline flow has been assumed, following the Hagen-Poiseuille formula, while actually the resistance is distributed along the whole length of the tube. Therefore, the above results are subject to experimental verification and correction. The salient conclusion, however, appears to be justified—that for minimum delay of response: (1) the volume of the pressure gauge should be as small as possible; (2) no concentrated resistance, in the form of damping capillary orifice, should be incorporated in the pneumatic system; (3) the tubing diameter should be in the neighborhood of that stated by the formula $d = 1.2 \times 10^{-3}\sqrt{L}$ (in which the dimensions are stated in meters).

Response to a Gradual Change of Air Speed

In the foregoing analysis a suddenly changing air speed has been assumed. With the aid of graphic analysis it is possible to determine the response to other than instantaneous changes, defined as a function of time. As an example, Fig. 10 illustrates the application of the method to a linear change of dynamic pressure, occurring in $2L/a$ time, in the pneumatic system treated in Fig. 5. It is seen that in this case the steps of the response function are not horizontal but slanting, forming a continuous broken line with decreasing slope toward the time-axis as time progresses.

With added labor but without any inherent difficulty, any other kind of pressure change, such as described by a curvilinear history function, can be analyzed with the graphic method described.

The method may be used for the solution of problems of other related aircraft instruments, such as altimeters and rate-of-climb indicators. Furthermore, it may applied to the analysis of engine pressure indicators and of the pressure fluctuation phenomena between two interconnected spaces, such as the main combustion chamber and the air cell of a Diesel engine. In the latter cases, however, the pressure difference is great; hence, the flow will not be laminar nor can the wave factor be regarded as a constant; therefore the procedure will be less simple than in the above-treated cases.

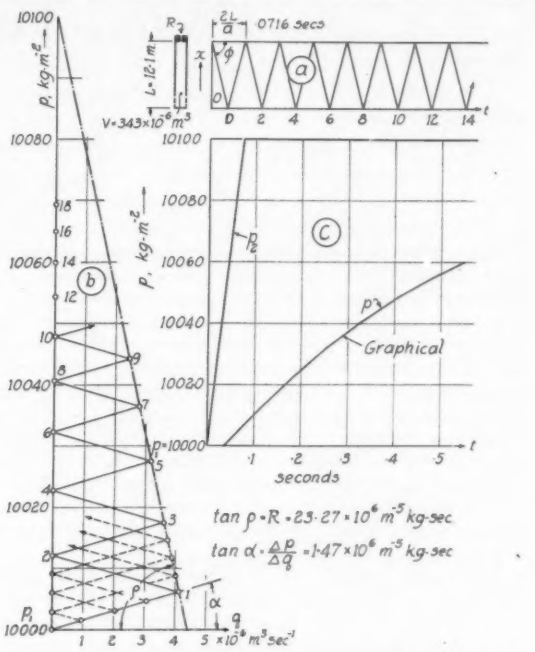

Fig. 10. Graphic analysis of Ju 52 air-speed indicator installation under the same assumptions as treated in Fig. 5, except that the impressed pressure change is assumed to be linear, rising from p_1 to p_2 during $2L/a$ time. (a) t-x diagram; (b) q-p diagram; (c) history diagram of pressure at pitot head, and at capsule (pressure rising from p_1 in a function of continuous slanting broken straight line, with the slope decreasing as time progresses).

References

[1] Beij, K. H., *Aircraft Speed Instruments*, N.A.C.A. T.R. No. 420, 1932.

[2] Weems, W. R., *The Effect of Tubing in the Indications of an Airspeed Meter*, Journal of the Aeronautical Sciences, Vol. 3, No. 5, pp. 165–167, March, 1936.

[3] Wildhack, W. A., *Pressure Drop in Tubing in Aircraft Instrument Installations*, N.A.C.A. T.N. No. 593, February, 1937.

[4] Eshbaugh, J. E., and Hoffman, E. L., *Examination of Lag in Air Speed Meters*, Army Air Forces Technical Report No. 1835.

[5] Weidemann, H., *Zur Traegheit von Staudruckanlagen*, Luftfahrtforschung, Vol. 17, No. 7, pp. 211–215, July 20, 1940; English translation under title: *Inertia of Dynamic Pressure Arrays*, N.A.C.A. T.M. No. 998.

[6] Oppelt, W., and Wenke, F., *Theoretische Betrachtung des Luftdruckvariometers und Richtlinien fuer Entwurf und Pruefung (Theoretical Treatment of the Rate of Climb Indicators and Principles for Its Design and Testing)*, Luftfahrtforschung, Vol. 14, No. 10, pp. 537–541, October 12, 1937.

[7] Schliestett, G. V., *Altitude Effects on an Uncompensated Rate-of-Climb Meter*, Journal of the Aeronautical Sciences, Vol. 6, No. 8, pp. 323–328, June, 1939.

[8] Draper, C. S., and Schliestett, G. V., *Dynamic Errors of the Rate-of-Climb Meter*, Journal of the Aeronautical Sciences, Vol. 5, No. 11, pp. 426–430, September, 1938.

[9] Brombacher, W. G., *Measurement of Altitude in Blind Flying*, N.A.C.A. T.N. No. 503, 1934.

[10] DeJuhasz, K. J., *Graphical Analysis of Transient Phenomena in Linear Flow*, Journal of The Franklin Institute, Vol. 223, No. 4, April, 1937; No. 5, May, 1937; No. 6, June, 1937. *Graphical Analysis of Surges in Mechanical Springs*, Journal of The Franklin Institute, Vol. 226, No. 4, October, 1938; No. 5, November, 1938; Vol. 227, No. 5, May, 1939. *Graphical Analysis of Transient Phenomena in Electric Circuits*, Journal of The Franklin Institute, Vol. 228, No. 3, September, 1939.

Wind-Tunnel Cooling

ARTHUR N. TIFFORD*
Curtiss-Wright Corporation

SUMMARY

The problem of cooling wind tunnels has been analyzed. It has been found that the turning vanes and the throat of the tunnel are the best places for using surface cooling.

As the operating speeds of tunnels increase, it becomes more and more difficult to cool the tunnel surfaces, and it becomes necessary to install a radiator in the tunnel. The detrimental effect of the use of a cooling radiator is small when the tunnel cross section is expanded ahead of the radiator. The percentage reduction in the energy ratio of the tunnel is given by the ratio of twice the adiabatic temperature rise, when the air in the radiator is brought to rest, to the temperature difference available for cooling, all multiplied by the ratio of the density of the air in the radiator to the density of the air in the throat of the tunnel.

The length-diameter ratio of the air passages of the cooler is determined by the cooling capacity required. The actual size of the air passages is limited, on the one hand, by the space available and, on the other, by the magnitude of the allowable power expenditure pushing the coolant through the radiator. The size of the radiator whose coolant power expenditure is equal to the power expended in the rest of the coolant circuit will, in general, be found to be about the best practical compromise.

INTRODUCTION

IN AN EFFORT to obtain large-scale, high-velocity data, the trend in modern wind-tunnel design has been toward larger tunnels operating at lower than atmospheric pressure. But as the size and power requirements of wind tunnels increase and as the operating pressures decrease, the problem of cooling becomes difficult. An examination of the literature reveals a noticeable lack of information on how to handle this difficult cooling problem. Furthermore, there is no information available on the relative merits of various practical solutions.

This paper attempts to supply some of this information by considering in detail the two most feasible methods of cooling wind tunnels: (1) cooling by heat transfer through the tunnel walls and/or the corner vanes; and (2) cooling by heat transfer to a radiator installed in the tunnel.

ANALYSIS

The following is an analysis of the available information applicable to wind-tunnel cooling.

The equation for heat transfer through a laminar boundary layer in a compressible fluid is[1]

$$(d/dt)[Jc_pT + (u^2/2)] = (k\partial^2/\partial y^2)[Jc_pT + (\sigma u^2/2)] \quad (1)$$

where

J = mechanical equivalent of heat
c_p = specific heat of fluid at constant pressure
T = temperature
u = velocity
k = thermometric conductivity
y = distance perpendicular to surface
σ = Prandtl number
t = time

In the case of heat transfer to a flat plate at a constant wall temperature, Eckert and Drewitz[2] found that when $\sigma = 1$, the heat transfer per unit surface per unit time is given by

$$H/S = \mu c_p(\partial T/\partial y)_0 = \mu[c_p(T_1 - T_W) + (u_1^2/2J)] \times (\partial u/\partial y)_0/u_1 \quad (2)$$

where the new symbols are defined as

H = heat dissipation
S = surface
μ = coefficient of absolute viscosity
$(\partial T/\partial y)_0$ = temperature gradient at surface
T_1 = temperature outside the boundary layer
T_W = temperature of surface
u_1 = velocity outside the boundary layer
$(\partial u/\partial y)_0$ = velocity gradient at surface

Eq. (2) should apply very closely for heat transfer from air ($\sigma = 0.73$) since the velocity and temperature fields in the boundary layer are very nearly the same when $\sigma = 0.73$ and when $\sigma = 1$. This solution is based on the Blasius velocity distribution in the boundary layer and therefore assumes no pressure drop across the plate. It may, however, be regarded as an approximate solution to the general heat-transfer equation when the pressure gradient along the plate is small. This approximate solution will now be put into a very convenient form for cooling calculations.

The pressure gradient at a given section of a wind tunnel is given by

$$\Delta p/L = \mu(\partial u/\partial y)_0(4/D)$$

where D is the diameter of the tunnel at the section considered.

Substituting this relation into Eq. (2), Eq. (3) is derived.

$$H = \{[(T_1 + u_1^2)/2Jc_p] - T_W\}(\pi D^2/4)\,\Delta p(c_p/u_1) \quad (3)$$

Assuming the average velocity at the section is approximated by u_1,

Received October 31, 1942.

* Aerodynamicist. Now, Chief Resident Engineer, Fedders Manufacturing Company.

$$H = \{[(T_a + u_a^2)/2Jc_p] - T_W\}c_pM\Delta p/\rho_a u_a^2 \quad (4)$$

where

ρ_a = the average air density at the section
u_a = the average velocity at the section
T_a = the average air temperature at the section

Eq. (4) is similar in form to the usual heat balance equation[3] encountered in dealing with heat transfer from an incompressible fluid to a wall at constant temperature.

$$H = (T_a - T_W)c_pM(1 - e^{-\Delta p/\rho_a u_a^2})$$

or at low values of $\Delta p/\rho_a u_a^2$

$$H = (T_a - T_W)c_pM\Delta p/\rho_a u_a^2 \quad (5)$$

When dealing with heat transfer from a compressible fluid to a wall at constant temperature, the usual heat balance equation (Eq. (5)) applies, provided the effective temperature of the fluid is taken as the actual fluid temperature plus the adiabatic temperature rise, $u_a^2/2Jc_p$, which occurs when the fluid is brought to rest. Because Reynolds analogy between the mechanism of heat transfer and friction applies to both laminar and turbulent air flow, Eqs. (4) and (5) are applicable in both cases.

Surface Cooling

Consider a closed return-circuit wind tunnel with small angles of expansion and contraction throughout. The flow through such a tunnel will be similar to turbulent flow in a long pipe. The frictional pressure drop is therefore approximated by the relation

$$\Delta pD/2\rho_a u_a^2 L = 0.049(\rho_a u_a D/\mu)^{-0.2} \quad (6)$$

which has been given by McAdams[4] as representing the frictional pressure drop in the latter case. The mass flow of air through the tunnel being constant, Eq. (6) can be put into the more convenient form

$$\Delta p/\rho_a u_a^2 = (0.098L/D^{0.8})(4M/\pi\mu)^{-0.2} \quad (7)$$

where the quantity in parenthesis is constant for all sections of the tunnel. Eq. (7) shows that the friction, $\Delta p/\rho_a u_a^2$, per unit length is inversely proportional to $D^{0.8}$. Because the heat dissipation is roughly proportional to $\Delta p/\rho_a u_a^2$ (Eq. 4), the greatest heat dissipation per unit length of tunnel will occur at the tunnel throat. Because the turning vanes of the tunnel form, in general, passages of smaller hydraulic diameter than the throat of the tunnel, the vanes offer the most effective surfaces for cooling.

In all well-designed wind tunnels, the working section occurs immediately after a rapid contraction in the tunnel cross-sectional area. Because of the resultant thinning of the boundary layer, the friction is more intense in the throat of wind tunnels than in long pipes. In other words, the throat of a tunnel is an even more efficient place at which to cool than the above analysis indicates. Similarly, because the passages between the turning vanes of the tunnel are analogous to the entrance length of a pipe,[5] they will have more friction and more cooling capacity than indicated above.

It has now been established that the working section and the turning vanes offer the best surfaces for cooling wind tunnels. The next question that arises is how much cooling surface will be needed.

When the cooling at the working section is sufficient to carry off the heat generated there, Eq. (8) applies.

$$Q\Delta p/J = [(T_a + \Delta T_a ad) - T_W](c_pM\Delta p/\rho_a u_a^2) \quad (8)$$

where Q is the volume flow of air. From Eq. (8) it is easily shown that the difference between the air temperature and the wall temperature must be equal to the adiabatic temperature rise of the air when brought to rest if sufficient cooling is to be obtained.

$$2\Delta T_a ad = (T_a + \Delta T_a ad) - T_W \quad (9)$$

Eq. (9) has not been further simplified because the temperature, $T_a + \Delta T_a ad$, is related to the temperature at which test models will be operating and is therefore limited by structural considerations.

Eq. (9) shows that as the speed at the test section of wind tunnels increases it becomes increasingly difficult to carry off by surface cooling the heat generated there. It is evident that, despite the reduction in the life of the turning vanes, they must be used for cooling in all large tunnels using surface cooling. The heat dissipation to be expected from the vanes can be estimated conservatively by the use of Eqs. (4) and (6) or, more exactly, by the use of Eq. (4) and the data for the inlet length of pipes given by Langhaar.[5]

Quite often even these two sets of surfaces—the working section and the turning vanes—will not be sufficient to handle all the cooling of the tunnel. In such cases the next most efficient surfaces for cooling—those where the tunnel has small cross-sectional areas—will have to be used.

Radiator Cooling

A wind tunnel can be cooled by means of a radiator installed in the tunnel instead of by surface cooling. In order to keep the power expended pushing air through the radiator and the turbulence of the tunnel at a minimum, the radiator should be carefully designed so as to have only frictional pressure losses. How much bad effect on the performance of a wind tunnel such a well-designed radiator would have is easily evaluated.

The performance of a wind tunnel is usually described by its energy ratio

$$\text{E.R.} = (Mu_t^2/2)/\text{power input} \quad (10)$$

where the subscript t refers to average air conditions in the throat of the tunnel. But all the power put into the tunnel eventually appears in the form of heat which must be carried off by the coolant system. For ade-

quate cooling, therefore, the heat balance of the wind tunnel is expressed by

$$Mu_t^2/2J/\text{E.R.} = \{[T_r + (u_r^2/2Jc_p)] - T_W\}(c_p M \Delta p/p_r u_r^2)$$

or

$$[(T_r + \Delta T_r ad)/(T_r + T_r ad)]^{1/\gamma-1}[2\Delta T_r ad \div (T_r + \Delta T_r ad) - T_W] = \text{E.R.}[\Delta p/(\rho_t u_t^2/2)] \quad (11)$$

where the subscript r refers to average air conditions in the radiator.

Eq. (11) states that the percentage reduction in the energy ratio of a wind tunnel due to the use of a radiator is equal to the ratio of twice the adiabatic temperature rise of the air in the radiator, when brought to rest, to the temperature difference available for cooling, all multiplied by the ratio of the density of the air in the radiator to the density of the air in the throat of the tunnel. Because the temperature, $T_r + \Delta T_r ad$, is limited by the allowable temperature of the model and the temperature T_W is limited by the coolant system, the percentage reduction in the energy ratio of the tunnel depends completely on the air speed in the radiator. In other words the reduction in the energy ratio of the tunnel can be made as small as desired by expanding the cross-sectional area of the tunnel ahead of the radiator.

The adiabatic temperature rise that occurs when the air flowing through the radiator is brought to rest is easily related to the adiabatic temperature rise equivalent of the air ahead of the radiator by the geometry of the cooler. Thus, in general, the open area of the radiator will be about half that of the tunnel cross section in which it is placed. It follows that the velocity of the air in the radiator will be twice that ahead of the radiator or the adiabatic temperature rise equivalent will be four times that ahead of the radiator. Eq. (11) can therefore be expressed in the more convenient form,

$$\frac{\text{E.R.}\,\Delta p}{\rho_t u_t^2/2} = \frac{\Delta\text{E.R.}}{\text{E.R.}} \backsimeq \left(\frac{T_r + \Delta T_r ad}{T_r + \Delta T_r ad}\right)^{\frac{1}{\gamma-1}} \times \frac{8\Delta T_r ad}{(T_r + \Delta T_r ad) - T_W} \quad (12)$$

where $\Delta T_r ad$ equals the adiabatic temperature rise equivalent of the air ahead of the radiator.

The loss in wind-tunnel performance due to the use of a radiator for cooling has now been evaluated. It has also been shown that in order to have adequate cooling, a definite value for $\Delta p/\rho_r u_r^2$ must be attained (Eq. 4). The value of $\Delta p/\rho_r u_r^2$ defines the geometry of the air passages of the cooler, i.e., the length-diameter ratio. The actual radiator depth, however, is a compromise between two factors: the space available and the magnitude of the power to be expended pushing the coolant through the radiator. The latter decreases inversely as the cube of the depth of the radiator. The optimum radiator depth will, in general, be approximated by the depth of the radiator whose coolant power expenditure is equal to the power expended in the rest of the coolant circuit.

Conclusions

The problem of cooling wind tunnels has been analyzed. It has been shown that as the operating speeds of tunnels increase (1) it becomes more and more difficult to cool the walls of the tunnel, and (2) in the absence of a radiator, the cooling of the turning vanes becomes mandatory. It has also been shown that the reduction in the energy ratio of the tunnel due to the use of a radiator can be made as small as desired by expanding the tunnel cross section ahead of the radiator.

In any plan for reducing the effect of the radiator installation on the performance of the wind tunnel by the use of a combination turning-vane-radiator design, the nonturbulent character of the flow will tend to be compromised. Furthermore, at its best the turning-vane-radiator is only equivalent, not superior, to an installation in which vane cooling plus radiator cooling is used. Because of the relative simplicity of construction of the latter, the turning-vane-radiator installation should not be given serious consideration.

References

[1] Goldstein, S., *Modern Developments in Fluid Dynamics*, Vol. II, p. 612; Oxford University Press, Great Britain, 1938.

[2] Eckert, E., and Drewitz, O., *Der Wärmeübergang an eine mit grober Geschwindigkeit längs angeströmte Platte*, Forschung auf dem gebiete des ingenieurwesens, Vol. 11, No. 3, pp. 116–122 May–June, 1940.

[3] Capon, R. S., *The Cowling of Cooling Systems*, R. & M. No. 1702, 1936.

[4] McAdams, W. H., *Heat Transmission*, p. 111; McGraw-Hill Book Co., Inc., 1933.

[5] Langhaar, H. L., *Steady Flow in the Transition Length of a Straight Tube*, Journal of Applied Mechanics, Vol. 9, No. 2, pp. 55–58, June, 1942.

The Influence of Sweep on the Spanwise Lift Distribution of Wings

F. THEILHEIMER*
Brown University

SUMMARY

A method is developed for determining the twist of a swept-back wing with prescribed spanwise lift distribution. Explicit formulas are derived for the case that the lift is given at eight points of the semispan.

INTRODUCTION

NUMEROUS METHODS for computing the spanwise lift distribution of a monoplane wing with arbitrary chord distribution have been worked out.[1] However, the lift distribution furnished by these methods agrees well with experimental results only if the line containing the centers of pressure of the wing sections (approximately the quarter chord line) is straight and at a right angle to the direction of flight. Sweep back of the wing increases the load at the wing tips. This effect has an unfavorable influence on the stalling characteristic of the wing unless it is compensated for by giving the wing a suitable twist.

The problems connected with the spanwise lift distribution of a swept-back wing are of twofold nature: Either the shape of a wing is given, and the lift distribution has to be found, or it may be asked what twist has to be given to a swept-back wing in order to get a certain lift distribution. The first problem is dealt with in papers by Crean[2] and by Weinig.[3] The present paper is devoted to the second problem, which may be formulated more precisely as follows: A straight wing with a certain lift distribution may be given sweep back by sliding each section back; then find the angle of attack at which the swept-back wing sections have to be placed in order to preserve the original lift distribution. For this new angle of attack a formula is found here, which expresses the angle in terms of the given lift distribution. In deriving this formula the present paper follows closely the procedure of Crean[2]; but whereas Crean's paper restricts itself to small angles of sweep back, no such restriction has been made here. Weinig[3] likewise assumes small sweep back and, furthermore, considers only wings with rectangular lift distribution.

The coordinate system is taken in the usual way: x-axis in the direction of flight, y-axis to starboard, z-axis downward. The wing is assumed to be symmetric with respect to the x-axis. The locus of the centers of pressure of the wing sections—approximately at one-quarter of the chord for wings without flaps—may be called the pressure line. Only wings with pressure lines consisting of two straight line segments in the x-y plane are considered here. The angle between a pressure line segment and the y-axis shall be called the angle of sweep Λ, taken positive for sweep back (see Fig. 1).

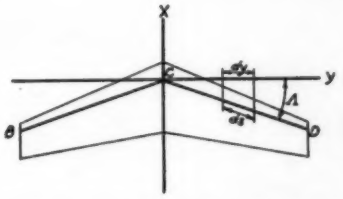

FIG. 1. Diagram of a swept-back wing. BCD = pressure line.

The theory of the lifting line can also be applied to the swept-back wing, the lifting line coinciding with the pressure line. A lifting line element of length ds and vorticity Γ along a pressure line swept back through an angle Λ (see Fig. 1) will experience a lift of

$$\rho\Gamma V \cos\Lambda \, ds$$

V being the velocity in the negative x-direction, and ρ being the density of the air. Since $dy = ds \cos\Lambda$, the lift of a wing section bounded by two planes perpendicular to the y-axis is

$$dL = \rho\Gamma V \, dy$$

The vorticity Γ is given by the following relation:

$$\Gamma = a_0 c V \alpha_0/2$$

where a_0 and c are section characteristics that are unchanged when the wing section is slid back; α_0 is the

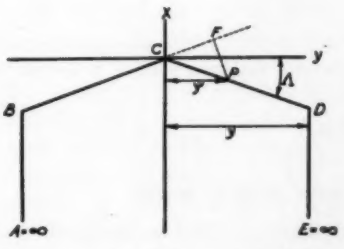

FIG. 2. A vortex of the swept-back wing.

Received December 10, 1942.

* This paper has been prepared under the direction of Prof. W. Prager while the author was a Fellow in the Program of Advanced Instruction and Research in Mechanics at Brown University (Academic year 1941–1942). The problem was suggested by The Glenn L. Martin Company.

effective angle of attack. The vorticity and likewise the lift distribution will therefore remain unaltered as long as the effective angle α_0 is not changed. This will be the case if

$$\alpha - (w/V) = \alpha_s - (w_s/V)$$

where α denotes the geometric angle of attack and w the down-wash velocity for the straight wing, while α_s and w_s are the values of these quantities for the swept-back wing. Thus the following result is found: By sweeping a wing back, the lift distribution will be preserved if the angle of attack of each wing section is changed by an angle α^*, which is given by

$$\alpha^* = \alpha_s - \alpha = (w_s - w)/V$$

This additional angle of attack will, of course, vary along the span.

The Down-Wash Velocity

The vortex system of the swept-back wing is a superposition of vortices of the type shown in Fig. 2. The down-wash velocity induced at a point P of the pressure line by the whole vortex system is the sum of the contributions that each individual vortex gives. A single vortex ABCDE of vorticity $-\Delta\Gamma$ induces at P the velocity

$$\Delta w_s = \frac{1}{4\pi}\left[\frac{1+\cos \mathrm{ABP}}{y+y'} + \frac{\cos \mathrm{PBC} + \cos \mathrm{BCP}}{PF} + \frac{\cos \mathrm{PDE} + 1}{y-y'}\right]\left(-\Delta\Gamma\right)$$

It can be seen from Fig. 2 that $\cos \mathrm{PDE} = -\sin\Lambda$; but that is the case only if $y' < y$, as in the figure; for $y' > y$, however, $\cos \mathrm{PDE} = +\sin\Lambda$. By using $|y-y'|$, the absolute value of $y-y'$, these two cases can be combined into one expression:

$$\cos \mathrm{PDE}/(y-y') = -\sin\Lambda/|y-y'|$$

and Δw_s becomes

$$\Delta w_s = \frac{1}{4\pi}\left[\frac{1}{y+y'}\left(1 - \frac{(y-y')\sin\Lambda}{\sqrt{y^2+2yy'\cos 2\Lambda + y'^2}}\right) + \frac{1}{2y'\sin\Lambda}\left(\frac{y+y'\cos 2\Lambda}{\sqrt{y^2+2yy'\cos 2\Lambda+y'^2}} - \cos 2\Lambda\right) - \frac{\sin\Lambda}{|y-y'|} + \frac{1}{y-y'}\right]\left(-\Delta\Gamma\right) = \frac{1}{4\pi}\left[\frac{1}{y+y'} - \frac{\cos 2\Lambda}{2y'\sin\Lambda} - \frac{\sin\Lambda}{|y-y'|} + \frac{1}{y-y'} + \frac{\sqrt{y^2+2yy'\cos 2\Lambda+y'^2}}{2y'\sin\Lambda(y+y')}\right]\left(-\Delta\Gamma\right)$$

Since the velocity induced by a straight wing of vorticity $-\Delta\Gamma$ is

$$\Delta w = (1/4\pi)\{[1/(y+y')] + [1/(y-y')]\}(-\Delta\Gamma)$$

the additional down-wash velocity due to sweep back is found to be

$$\Delta w_s - \Delta w = \frac{1}{4\pi}\left[-\frac{\cos 2\Lambda}{2y'\sin\Lambda} - \frac{\sin\Lambda}{|y-y'|} + \frac{\sqrt{y^2+2yy'\cos 2\Lambda+y'^2}}{2y'\sin\Lambda(y+y')}\right]\left(-\Delta\Gamma\right) = \frac{1}{4\pi}\left[-\frac{1}{2uy'} + u\left(\frac{1}{y'} - \frac{1}{|y-y'|}\right) + \frac{\sqrt{y^2+2yy'+y'^2-4yy'u^2}}{2y'u(y+y')}\right](-\Delta\Gamma)$$

where u was written for $\sin\Lambda$.

The term $\sqrt{(y^2+2yy'+y'^2-4yy'u^2)}/2y'u(y+y')$ can be expanded into a series:

$$\frac{1}{2y'u}\sqrt{1 - \frac{4yy'u^2}{(y+y')^2}} = \frac{1}{2y'u}\left[1 - \sum_{n=1}^{\infty} C_n\left(\frac{4yy'u^2}{(y+y')^2}\right)^n\right]$$

where $C_n = [1\cdot 1\cdot 3, \ldots (2n-3)]/[2\cdot 4\cdot 6, \ldots 2n]$. In this series each term is less than half the preceding one if $u^2 \leqq 1/2$ or $\Lambda \leqq 45°$. The numerical computations will show that the terms for $n = 2$ and $n = 3$ are already small; therefore, the terms for $n > 3$ shall be neglected, so that $\Delta w_s - \Delta w$ can be written as follows:

$$\Delta w_s - \Delta w = \frac{1}{4\pi}\left[u\left(\frac{1}{y'} - \frac{1}{|y-y'|} - \frac{y}{(y+y')^2}\right) - u^3\frac{y^2y'}{(y+y')^4} - u^5\frac{2y^3y'^2}{(y+y')^6}\right]\left(-\Delta\Gamma\right)$$

The Additional Angle of Attack

The vortex system shall be assumed to consist of N vortices. Let y_{2m+1}, $m = 0, \ldots, N-1$, be the span coordinates of the points where these vortices branch off the pressure line. Then the down-wash velocity shall be

computed at $N-1$ points y_{2k}, $k = 1, \ldots, N-1$, which lie between the branching-off points of the vortices. If the vorticity for the points y_{2k} is given, the vorticity of the vortex branching off at y_{2m+1} is

$$-\Delta\Gamma = \Gamma(y_{2m}) - \Gamma(y_{2m+2})$$

where it is assumed that $\Gamma(0)$ is also given and that $\Gamma(b/2) = 0$, b being the span. Thus the additional downwash velocity due to sweep back induced at y_{2k} by the whole vortex system can be written as a sum:

$$w_s - w = \frac{1}{4\pi}\sum_{m=0}^{N-1}\left[u\left(\frac{1}{y_{2k}} - \frac{1}{|y_{2m+1} - y_{2k}|} - \frac{y_{2m+1}}{(y_{2m+1} + y_{2k})^2}\right) - u^3\frac{y_{2m+1}^2 y_{2k}}{(y_{2m+1} + y_{2k})^4} - u^5\frac{2y_{2m+1}^3 y_{2k}^2}{(y_{2m+1} + y_{2k})^6}\right]\left[\Gamma(y_{2m}) - \Gamma(y_{2m+2})\right]$$

Dividing this expression by V, the additional angle of attack α^* is obtained. Introducing dimensionless coordinates $\eta = y/(b/2)$ and dimensionless circulation coefficients $\gamma = \Gamma/Vb$ and putting $\gamma(\eta_{2m}) = \gamma_m$, the additional angle of attack α^* for the point η_{2k} is found to be

$$\alpha^*(\eta_{2k}) = \sum_{m=0}^{N-1}(a_{mk}u - b_{mk}u^3 - c_{mk}u^5)(\gamma_m - \gamma_{m+1})$$

where

$$a_{mk} = \frac{1}{2\pi}\left[\frac{1}{\eta_{2k}} - \frac{1}{|\eta_{2m+1} - \eta_{2k}|} - \frac{\eta_{2m+1}}{(\eta_{2m+1} + \eta_{2k})^2}\right]$$

$$b_{mk} = (1/2\pi)[\eta_{2m+1}^2\eta_{2k}/(\eta_{2m+1} + \eta_{2k})^4]$$

$$c_{mk} = (1/\pi)[\eta_{2m+1}^3\eta_{2k}^2/(\eta_{2m+1} + \eta_{2k})^6$$

This, in turn, can be simplified by putting

$$f_{0k} = a_{0k};\quad f_{mk} = a_{mk} - a_{m-1,k}$$

$$g_{0k} = b_{0k};\quad g_{mk} = b_{mk} - b_{m-1,k}$$

$$h_{0k} = c_{0k};\quad h_{mk} = c_{mk} - c_{m-1,k},\ m = 1, \ldots, N-1$$

Thus, $\alpha^*(\eta_{2k})$ becomes

$$\alpha^*(\eta_{2k}) = \sum_{m=0}^{N-1}(f_{mk}u - g_{mk}u^3 - h_{mk}u^5)\gamma_m$$

or

$$\alpha^*(\eta_{2k}) = F_k\sin\Lambda - G_k\sin^3\Lambda - H_k\sin^5\Lambda \tag{1}$$

where

$$F_k = \sum_{m=0}^{N-1} f_{mk}\gamma_m \qquad G_k = \sum_{m=0}^{N-1} g_{mk}\gamma_m \qquad H_k = \sum_{m=0}^{N-1} h_{mk}\gamma_m \tag{2}$$

The structure of Eqs. (1) and (2) shows that in order to find α^* at the $N-1$ points η_{2k}, $k = 1, \ldots, N-1$, it is necessary to compute only once the coefficients f_{mk}, g_{mk}, and h_{mk}. Then the values F_k, G_k, and H_k for any arbitrary lift distribution are obtained by inserting the circulation coefficients γ_m of that lift distribution into Eqs. (2), and α^*—in radians—is given by Eq. (1) in terms of the angle of sweep back Λ.

Numerical Work

The computation of the coefficients f_{mk}, g_{mk}, and h_{mk} was carried out for the case that the vorticity is prescribed at the eight points of the semispan whose coordinates are $\eta_{2m} = \sin(m\pi/16)$, $m = 0, \ldots, 7$. The coordinates $\sin[(2m+1)\pi/32]$ were chosen as η_{2m+1}. The coefficients f_{mk}, g_{mk}, and h_{mk}, $m = 0, \ldots, 7$; $k = 1, \ldots, 7$, are tabulated in Table 1, so that α^* can readily be obtained by means of Eqs. (1) and (2) if the eight circulation coefficients $\gamma_0, \ldots, \gamma_7$ are assigned. For a set of values γ_m, which were kindly given by The Glenn L. Martin Company, the coefficients F, G, and H are tabulated in Table 2, and the angle α^*—in degrees—for angles of sweep back $\Lambda = 15°$ and $30°$ is plotted in Fig. 3.

TABLE 1

m ↓	$k \to 1$	2	3	4	5	6	7
				f_{mk}			
0	−1.0054	−0.2107	−0.09788	−0.06028	−0.04364	−0.03538	−0.03142
1	−0.04691	−1.1978	−0.2823	−0.14290	−0.09575	−0.07768	−0.06539
2	1.1232	−0.07217	−1.2954	−0.3009	−0.15541	−0.10494	−0.08893
3	0.2358	1.1669	−0.12825	−1.5158	−0.3684	−0.2011	−0.15015
4	0.10247	0.2299	1.3045	−0.2263	−1.9156	−0.5063	−0.3093
5	0.05382	0.09330	0.2301	1.5052	−0.4323	−2.7384	−0.8427
6	0.02907	0.04455	0.09250	0.2740	1.8864	−1.0211	−5.0635
7	0.01295	0.01874	0.03520	0.08491	0.2964	2.5820	−4.3869
				g_{mk}			
0	0.04042	0.01096	0.004656	0.002573	0.001704	0.001295	0.001107
1	0.006723	0.01406	0.009831	0.007009	0.005339	0.004258	0.003932
2	−0.012190	0.000358	0.003178	0.003382	0.003163	0.003068	0.002761
3	−0.008555	−0.002515	0.000083	0.001020	0.001329	0.001415	0.001431
4	−0.005308	−0.002468	−0.000789	0.000027	0.000396	0.000561	0.000619
5	−0.003139	−0.001878	−0.000852	−0.000283	0.000011	0.000158	0.000236
6	−0.001806	−0.001203	−0.000635	−0.000288	−0.000097	0.000005	0.000054
7	−0.000823	−0.000581	−0.000329	−0.000167	−0.000073	−0.000023	0.000002
				h_{mk}			
0	0.01799	0.003558	0.001187	0.000550	0.000321	0.000225	0.000183
1	0.004672	0.008717	0.005328	0.003404	0.002380	0.001769	0.001593
2	−0.008196	0.000265	0.002257	0.002269	0.002012	0.001863	0.001644
3	−0.004972	−0.001817	0.000062	0.000749	0.000950	0.000987	0.000983
4	−0.002715	−0.001686	−0.000583	0.000020	0.000294	0.000412	0.000450
5	−0.001546	−0.001221	−0.000614	−0.000210	0.000008	0.000118	0.000175
6	−0.000783	−0.000746	−0.000457	−0.000212	−0.000073	0.000004	0.000040
7	−0.000343	−0.000356	−0.000217	−0.000123	−0.000055	−0.000018	0.000001

TABLE 2

η	γ	F	G	H
0	0.3709	....	....	....
0.1951	0.3505	0.07361	0.008829	0.003227
0.3827	0.3169	−0.11257	0.007196	0.003154
0.5556	0.2792	−0.20497	0.005715	0.002687
0.7071	0.2400	−0.29460	0.004657	0.002244
0.8315	0.1998	−0.43062	0.003952	0.001912
0.9239	0.1536	−0.71476	0.003504	0.001691
0.9808	0.0931	−1.5335	0.003267	0.001570

CONCLUSIONS

The additional angle of attack α^* through which each swept-back wing section has to be turned in order to preserve the original lift distribution, was found to depend only on that lift distribution and, of course, on the angle of sweep back. Thus, if two straight wings have the same lift distribution but otherwise differ in section characteristics, they will, if swept back, lead to the same α^*.

The additional angle of attack is positive near the root of the wing and negative near the tip. This was to be expected, since sweep back causes a decrease in lift near the root and an increase near the tip and, to compensate for that, the angle of attack has to be changed accordingly.

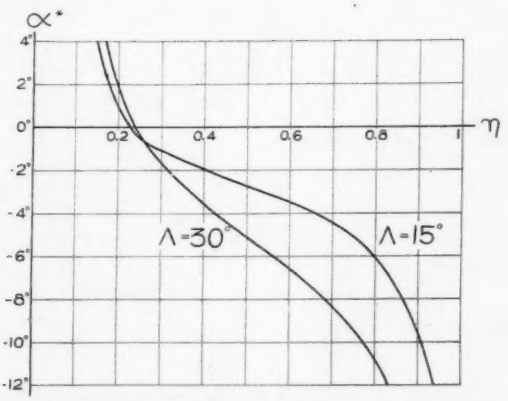

FIG. 3. Additional angle of attack α^* for angles of sweep back $\Lambda = 15°$ and $30°$.

REFERENCES

[1] U.S. Bureau of Air Commerce, *Spanwise Air-Load Distribution*, Washington, 1938, ANC-1 (1).

[2] Crean, J. R., *Monoplane Wings with Sweep—Theoretical Calculation of the Spanwise Lift Distribution*, Aircraft Engineering, Vol. 10, pp. 245–247, 1938.

[3] Weinig, F., *Schiebende und gepfeilte Tragflügel*, Luftfahrtforschung, Vol. 14, pp. 45–54, 1937.